AMERICAN SOCIETY FOR MICROBIOLOGY | Journal of Virology®

VIRUS-CELL INTERACTIONS

Rotavirus Induces Formation of Remodeled Stress Granules and P Bodies and Their Sequestration in Viroplasms To Promote Progeny Virus Production

Poonam Dhillon,[a] C. Durga Rao[a]

[a]Department of Microbiology & Cell Biology, Indian Institute of Science, Bangalore, India

ABSTRACT Rotavirus replicates in unique virus-induced cytoplasmic inclusion bodies called viroplasms (VMs), the composition and structure of which have yet to be understood. Based on the analysis of a few proteins, earlier studies reported that rotavirus infection inhibits stress granule (SG) formation and disrupts P bodies (PBs). However, the recent demonstration that rotavirus infection induces cytoplasmic relocalization and colocalization with VMs of several nuclear hnRNPs and AU-rich element-binding proteins (ARE-BPs), which are known components of SGs and PBs, suggested the possibility of rotavirus-induced remodeling of SGs and PBs, prompting us to analyze a large number of the SG and PB components to understand the status of SGs and PBs in rotavirus-infected cells. Here we demonstrate that rotavirus infection induces molecular triage by selective exclusion of a few proteins of SGs (G3BP1 and ZBP1) and PBs (DDX6, EDC4, and Pan3) and sequestration of the remodeled/atypical cellular organelles, containing the majority of their components, in the VM. The punctate SG and PB structures are seen at about 4 h postinfection (hpi), coinciding with the appearance of small VMs, many of which fuse to form mature large VMs with progression of infection. By use of small interfering RNA (siRNA)-mediated knockdown and/or ectopic overexpression, the majority of the SG and PB components, except for ADAR1, were observed to inhibit viral protein expression and virus growth. In conclusion, this study demonstrates that VMs are highly complex supramolecular structures and that rotavirus employs a novel strategy of sequestration in the VM and harnessing of the remodeled cellular RNA recycling bins to promote its growth.

IMPORTANCE Rotavirus is known to replicate in specialized virus-induced cytoplasmic inclusion bodies called viroplasms (VMs), but the composition and structure of VMs are not yet understood. Here we demonstrate that rotavirus interferes with normal SG and PB assembly but promotes formation of atypical SG-PB structures by selective exclusion of a few components and employs a novel strategy of sequestration of the remodeled SG-PB granules in the VMs to promote virus growth by modulating their negative influence on virus infection. Rotavirus VMs appear to be complex supramolecular structures formed by the union of the triad of viral replication complexes and remodeled SGs and PBs, as well as other host factors, and designed to promote productive virus infection. These observations have implications for the planning of future research with the aim of understanding the structure of the VM, the mechanism of morphogenesis of the virus, and the detailed roles of host proteins in rotavirus biology.

KEYWORDS rotavirus, viroplasm, stress granules, SGs, P bodies, PBs, AU-rich element-binding proteins, ARE-BPs, sequestration, colocalization, relocalization, remodeled/atypical SGs and PBs, liquid droplets

Received 7 August 2018 **Accepted** 20 September 2018

Accepted manuscript posted online 26 September 2018

Citation Dhillon P, Rao CD. 2018. Rotavirus induces formation of remodeled stress granules and P bodies and their sequestration in viroplasms to promote progeny virus production. J Virol 92:e01363-18. https://doi.org/10.1128/JVI.01363-18.

Editor Terence S. Dermody, University of Pittsburgh School of Medicine

Address correspondence to C. Durga Rao, cdrmcb@gmail.com.

Rotavirus, a leading cause of acute gastroenteritis in infants and young children worldwide, belongs to the family *Reoviridae*. Its genome consists of 11 segments of double-stranded RNA (dsRNA) enclosed in a triple-layered particle (TLP) and encodes six structural viral proteins (VPs) and six nonstructural proteins (NSPs) (1, 2). The inner capsid is formed by VP2, the intermediate capsid by VP6, and the outer capsid by VP4 and VP7 (3, 4). While VP4 and VP7 determine the serotype antigenic specificity, VP6 determines the subgroup antigenic specificity of rotavirus (5, 6).

Rotavirus infection induces the formation of unique electron-dense, cytoplasmic, nonmembranous structures called viroplasms (VMs), which are the specialized sites of viral genome replication and assembly of immature double-layered particles (DLPs) (1, 7–10). However, the detailed composition and structural organization of VMs have yet to be understood. Recently, Dhillon et al. (11) demonstrated that VMs are associated with a large number of nuclear hnRNPs (11–15), AU-rich element-binding proteins (ARE-BPs) (16–18), and cytoplasmic proteins, which either inhibit or promote virus growth. Association of the components of lipid droplets with VMs and their positive role in virus growth were also recently reported (19–21). VMs are formed during the early stages of rotavirus infection, nucleated by two essential nonstructural proteins, NSP2 and NSP5, and the inner capsid protein VP2. NSP5 is essential for the recruitment of the viroplasmic proteins and the architectural assembly of VMs (7–10, 22–24).

In response to various types of stress, including virus infection, eukaryotic cells have evolved different strategies to limit cellular damage during stress by regulating translation and mRNA turnover. A general and major cellular defensive response mechanism by which the cell limits damage against stress is through shutting off protein synthesis by phosphorylation of the eukaryotic initiation factor 2α (eIF2α) at Ser-51 by the stress-sensing kinases (25–30), triggering rapid translational arrest, polysome disassembly, molecular triage, and assembly of large, nonmembranous, cytoplasmic ribonucleoprotein complexes called stress granules (SGs) and of mRNA processing bodies (P bodies [PBs]) containing translationally stalled 48S preinitiation mRNA-protein (mRNP) complexes and other mRNA-associated factors (29–32). SG and PB formation during stress reprograms host protein synthesis for preferred translation of transcripts of genes associated with long-term cell survival and antiapoptotic signaling pathways (29, 30, 33, 34). SGs are also formed in a manner independent of eIF2α phosphorylation, including overexpression of some of the SG markers, such as the Ras-GTPase activating protein (SH3 domain)-binding protein1 (G3BP1) and TIA1/TIAL-1 (29, 30, 33–35).

SG assembly is finely regulated by the interaction of the two SG-nucleating and -resident proteins, i.e., G3BP1 and Caprin1 (35–40). SGs can also be formed without the requirement of G3BP1/2 and Caprin1, suggesting that the SG composition and mechanism of assembly can be context specific and that SGs may have different functions under different stress conditions (38, 41). Besides G3BP1 and Caprin1, SGs contain a large number of RNA-binding proteins, translation initiation factors, and signaling molecules (16–18, 29–34, 42–53).

In contrast to the stress-induced assembly of SGs, some PBs may be observed in unstressed cells. PBs include components of cytoplasmic deadenylase complexes, nonsense-mediated decay (NMD)-associated Upf proteins, ARE-binding proteins (ARE-BPs) (33, 34, 42–56), DCP bodies (consisting of the decapping machinery components) (42, 57–61), and GW bodies, associated with mRNA silencing, surveillance, and decay, that contain two highly conserved families of proteins (GW-rich/trinucleotide repeat-containing gene 6 protein [GW182/TNRC6] and Argonauts [Ago]) which form the core components of the microRNA-induced silencing complex (miRISC) (42, 52, 53, 62–66).

SGs range in size from being below the limit of detection in unstressed cells to being several micrometers across under conditions of stress (29). Both PBs and SGs are dynamic and are often observed in close proximity to one another, resulting in fusion and exchange or sharing of their protein and RNA components. Some components, except the core nucleating factors, were reported to be shared between SGs and PBs, but their constituents and functions may vary with the type of stress (34, 42–53, 63). Being in dynamic transition, SGs and PBs serve as sites for mRNP remodeling and can

TABLE 1 Summary of interactions between viroplasmic proteins and SG and PB proteins and of properties of endogenous SG and PB proteins[a]

Protein	Localization	Pulldown assay result or interaction				Colocalization with VM	Total protein level	Reference(s)
		RNase-untreated cells		RNase-treated cells				
		NSP5	NSP2	NSP5	NSP2			
ADAR1	SG	ND	ND	ND	ND	+	NSC	This study; 44, 79–81
Ago2	PB*	+	±	+	−	+	↓	This study; 44, 54
Caf1-p150	PB	−	±	−	−	+	↑	This study; 44, 54
Caprin1	SG	+	−	+	−	+	↑	This study; 40, 44, 50
CPEB	SG*	ND	ND	ND	ND	+	NSC	This study; 44, 63
DCP1a	PB (DCP)	+	+	+	+	+	NSC	This study; 44
DCP1b	PB (DCP)	+	+	+	+	±	NSC	This study; 44
DDX6	PB (DCP)	+	+	+	+	+ (R)	↑	This study; 44, 63
EDC4	PB (DCP)	+	+	+	+	+ (R)	↓	This study; 44, 58, 66
eIF2α	SG	+	+	−	+	+	↑	This study; 44
G3BP1	SG	−	−	−	−	−	NSC	This study; 11, 35, 44, 63
GW182	PB	+	+	+	+	+	↑	This study; 44
LSM1	PB	ND	ND	ND	ND	+	ND	This study; 44, 50
Pan3	PB (DCP)	−	−	−	−	−	ND	This study; 44
PPM1A	SG	ND	ND	ND	ND	+	↑	This study; 83, 87, 88
PKR	SG	+	−	+	−	+	↑	This study; 44
XRN1	PB (DCP)	+	+	+	+	+	↑	This study; 44, 55

[a]The interactions between the SG and PB proteins and the viral proteins NSP2 and NSP5 were identified by PD assays using RNase-treated and untreated MA104 control cell extracts followed by WB analysis, and colocalization of the proteins was identified by ICM analysis. +, positive interaction/colocalization; −, no interaction/colocalization; ±, weak interaction/partial colocalization/weak granule formation; R, reported to be shared/exchanged between SGs and PBs; DCP, present in distinct DCP bodies/granules; ND, not determined; NSC, no significant change; *, shared between SGs and PBs; ↑ and ↓, increased and decreased host protein levels, respectively, in virus-infected cells compared to those in uninfected cells.

be considered mRNP recycling/modification bins, as the translationally stalled mRNAs stored in the SGs can later be released either for translation under favorable conditions or for degradation via transition into PBs under persistently unfavorable conditions, depending on the physiological state of the cell (34, 42, 48). Different viruses either inhibit or induce SG and PB formation or cause vacillation in their assembly during the course of infection. Modulation of SGs and PBs and hijacking of their specific components for virus replication and/or protein synthesis represent an emerging field of interest (29, 42, 47, 50, 67–69).

In recent studies using three SG markers, TIA1, S6, and eIF4E, Montero et al. (70) reported that SGs are not formed in rotavirus-infected cells. Using G3BP1 as an SG marker, Dhillon et al. (11) also observed a lack of typical SG formation during rotavirus infection. Further, by analyzing three decapping complex proteins of PBs, namely, XRN1, Pan3, and DCP1a, Bhowmick et al. reported that PBs were disrupted in rotavirus-infected cells (71). However, the recent demonstration by Dhillon et al. (11) that several ARE-BPs, which are known components of SGs/PBs (16–18, 42–46), relocalize to the cytoplasm, exist in punctate structures, and colocalize with VMs in rotavirus-infected cells prompted us to investigate the status of SGs and PBs by analyzing a large number of their components to understand if rotavirus induces remodeling of SGs and PBs by selective dissociation of a few of their components and sequestration of the remodeled/atypical granules in the VM in virus-infected cells.

RESULTS

Immunofluorescence confocal microscopy (ICM) analyses reveal that the majority of SG and PB components are present in punctate structures that colocalize with VMs in rotavirus-infected cells. Several SG and PB proteins that were examined in this study are listed in Table 1. Examination of the known SG factors, such as dsRNA adenosine deaminase 1 (ADAR1), Caprin1, cytoplasmic polyadenylation element-binding protein (CPEB), eIF2α, 4E-binding protein 1 (4EBP1), dsRNA-dependent protein kinase (PKR), and Staufen1, at 8 h postinfection (hpi) surprisingly revealed their presence in punctate structures and colocalization with the VM (Fig. 1a and b), similar to the results reported recently for several ARE-BPs (11) in infected cells. While ADAR1 and

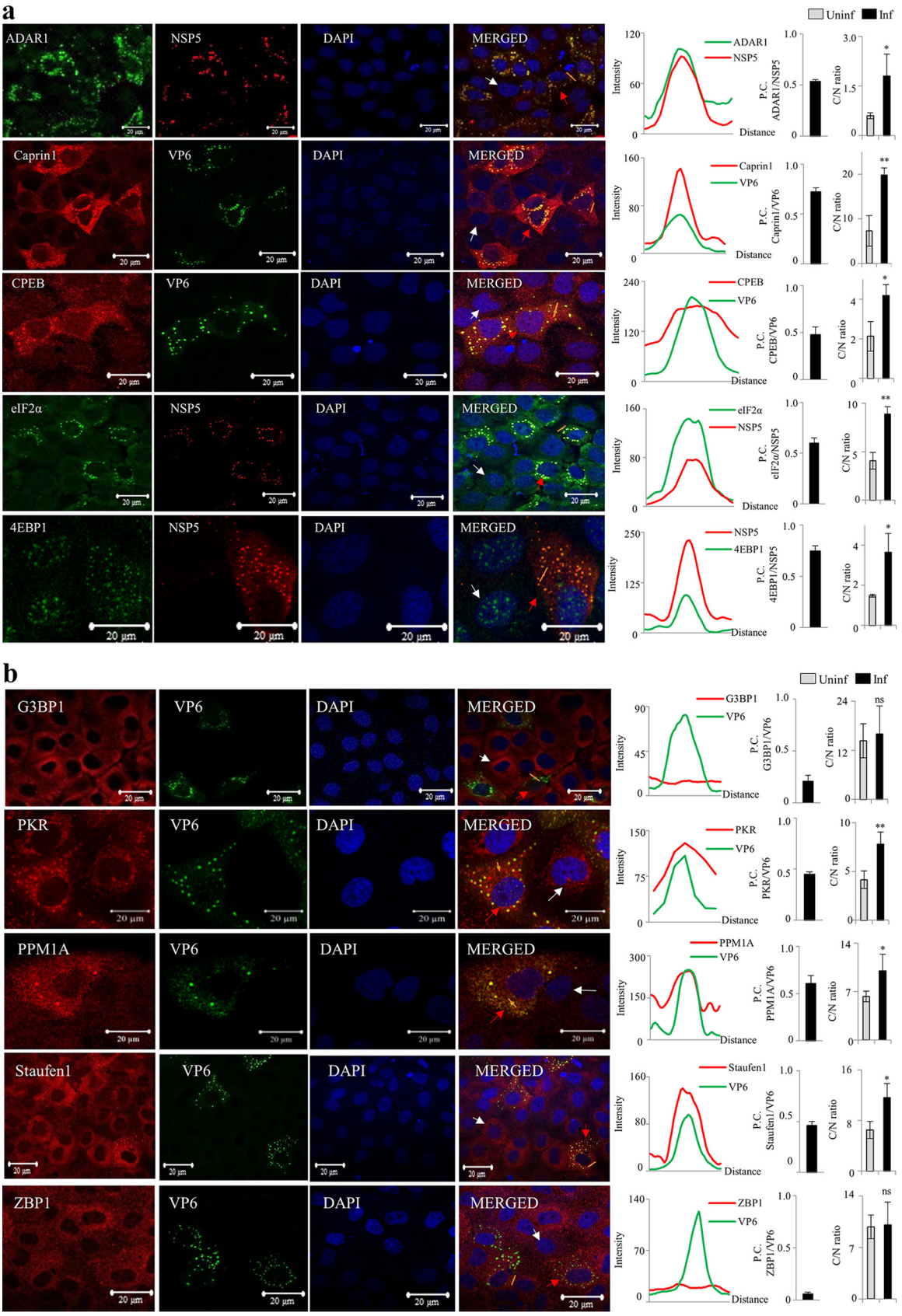

FIG 1 ICM analysis of formation of cytoplasmic granules by the majority of SG proteins and their colocalization with VMs in RRV-infected MA104 cells. (a and b) Formation of atypical SG granules and their colocalization with VM in RRV-infected cells. MAbs or PAbs against

(Continued on next page)

4EBP1 were located predominantly in the nucleus, both were present at detectable levels in the cytoplasm of the uninfected cells (Fig. 1a), but rotavirus infection induced their cytoplasmic relocalization and sequestration in the VMs. Further, 4EBP1 was detectable in the cytoplasm of serum-grown control cells and formed punctate structures in both the nucleus and the cytoplasm in the absence of serum in the uninfected cells present along with the infected cells on the same slide. The metal-dependent protein phosphatase M (PPM1A/PP2Cα) not only showed colocalization in the VMs but also was abundantly present in the cytoplasm (Fig. 1b). The eIF2α protein appeared to be present in both the nucleus and the cytoplasm and showed cytoplasmic accumulation and localization in the VM in infected cells, which appeared to be specific based on the location at identical sites of the punctate structures of the endogenous protein and the VM (Fig. 1a). As reported by Dhillon et al. (11) and as shown in Fig. 1b, G3BP1 and the Z DNA-binding protein (ZBP1) did not form punctate structures but exhibited a dispersed distribution in the cytoplasm of both the uninfected and virus-infected cells.

Analysis of several PB-associated proteins, namely, AGO2, GW182 (TNRC6A and TNRC6B), chromatin assembly factor 1 (Caf1-p150 and Caf1-p60), U6 snRNA-associated Sm-like protein 1 (LSM-1), and poly(A)-specific RNase (PARN), revealed that all these proteins were present in punctate structures in the virus-infected MA104 cells and colocalized with the VMs (Fig. 2). Unlike 4FBP1, which assumed punctate structures in both compartments in the absence of serum, the majority of the SG proteins and PB components (excluding the DCP granule proteins shown in Fig. 3) that were examined in this study exhibited a diffuse distribution in the nucleus and/or cytoplasm in the serum-grown control cells (not shown) similar to that observed in the uninfected cells (Fig. 1a and b and Fig. 2).

The fluorescence quantification of cytoplasmic/nuclear (C/N) ratios of abundance for the host proteins in the uninfected and infected cells on the same slide, with the uninfected cells serving as appropriate controls, and Pearson's coefficients for colocalization of host and viral proteins in the rhesus monkey rotavirus (RRV)-infected cells under the serum-lacking conditions of virus infection are shown in bar diagrams in the rightmost panels of Fig. 1a and b and Fig. 2.

Note that all the polyclonal antibodies (PAbs) against the host proteins and the secondary antibodies were screened for cross-reactivity with viral proteins by Western blotting (WB) and enzyme-linked immunosorbent assay (ELISA), using infected cell lysates, and only those that did not show cross-reactivity with viral proteins were used in this study.

Differential intracellular dynamics of decapping complex proteins. Interestingly, the decapping complex proteins, such as DEAD box helicase 6 (DDX6/RCK/p54), enhancer of mRNA decapping 4 (EDC4/Ge-1/HEDL), decapping enzyme components DCP1a and DCP1b, 5′-3′ exoribonuclease XRN1 (57–61), and poly(A)-specific RNase subunit Pan3 (42, 48, 54–56), existed in distinct subsets of PB granules (called DCP bodies) in the cytoplasm of serum-grown control cells, with all six decapping complex proteins colocalizing with each other in the same granules (Fig. 3a). In this context, the existence of the decapping complex proteins in DCP bodies, whose composition may

FIG 1 Legend (Continued)
different SG proteins, affinity-purified PAb against NSP5, an SGI-specific anti-RRV DLP MAb against VP6, and Cy3-tagged anti-mouse (green) and Cy5-tagged anti-rabbit (red) IgG secondary antibodies were used. MA104 cells were grown on coverslips and infected for 8 h with RRV at an MOI of 0.5. The cells were incubated with appropriate antibodies, and after mounting in DAPI (4′,6-diamidino-2-phenylindole), the proteins were visualized by fluorescence microscopy under an LSM Zeiss 710 or LSM 880 immunofluorescence confocal microscope (63×; oil immersion) as recently described (11). Uninfected and infected cells are indicated by white and red arrows, respectively, and the plot profile path on the VM is indicated by an orange line. Pearson's coefficients (P.C.) were calculated to assess the colocalization of viral proteins (NSP5/VP6) and SG/PB proteins in RRV-infected cells. The values represent averages for 50 infected cells, and the error bars indicate standard deviations (SD). Fluorescence quantification of each of the host proteins over whole cells was carried out on 50 infected and 50 uninfected cells from the same slide, and arithmetic averages ± SD were calculated. Average C/N ratios from three independent experiments were also calculated, and the data from one of the experiments are shown. Quantification of the cytoplasmic/nuclear ratio of the proteins was done using ImageJ software. Uninf, uninfected cells (gray bars); Inf, infected cells (black bars). Significance was calculated using Student's *t* test. *, $P < 0.05$; **, $P < 0.01$; ***, $P < 0.001$; ns, not significant.

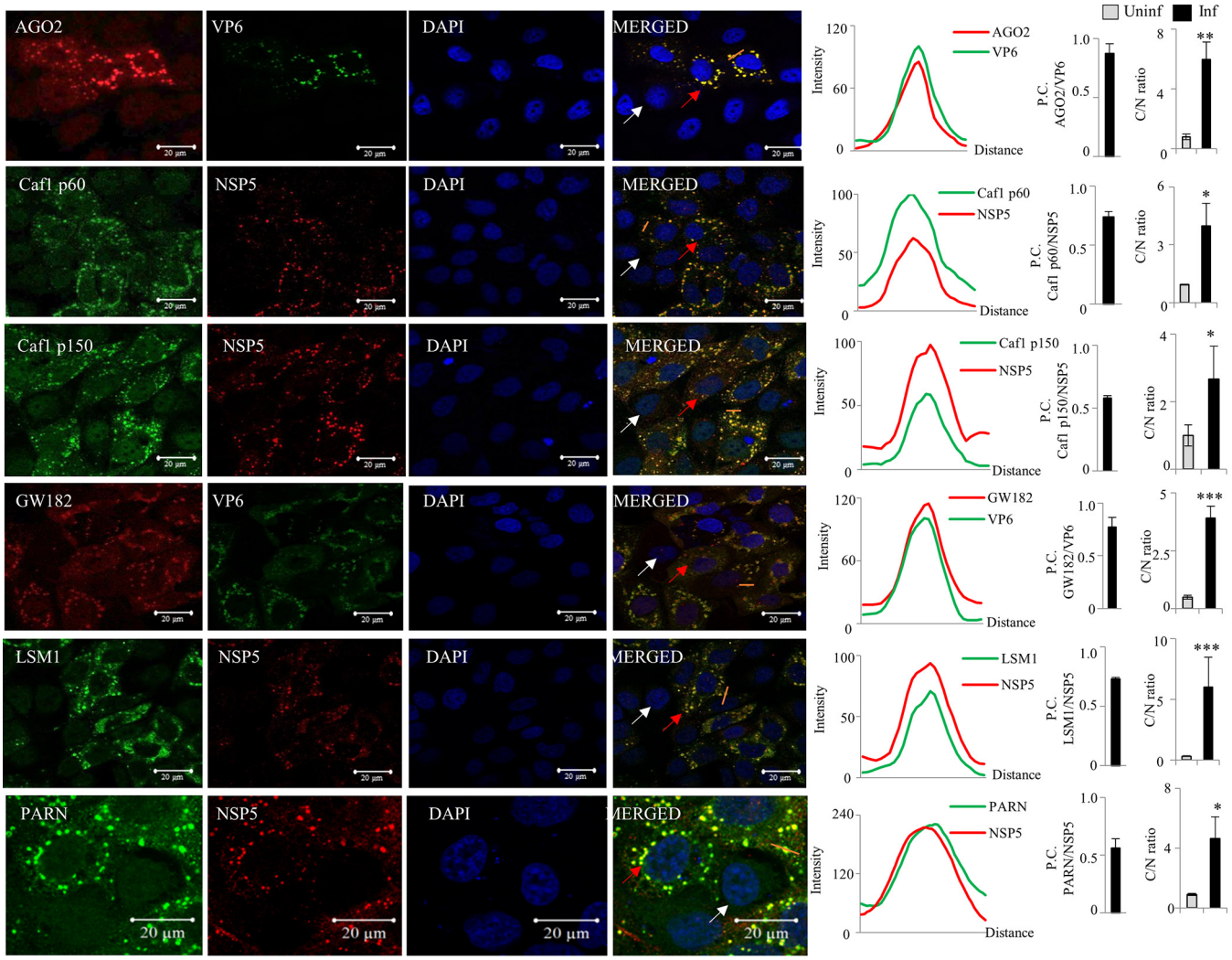

FIG 2 Demonstration by ICM of the existence of the majority of the PB proteins in granule structures and their colocalization with VM in RRV-infected cells. MAbs or PAbs against different PB proteins, affinity-purified PAb against NSP5, an SGI-specific anti-RRV DLP MAb against VP6, and Cy3-tagged anti-mouse (green) and Cy5-tagged anti-rabbit (red) IgG secondary antibodies were used. MA104 cells were grown on coverslips and infected for 8 h with RRV at an MOI of 0.5. Uninfected and infected cells are shown by white and red arrows, respectively. The plot profile path on the VM is indicated by an orange line. Fluorescence quantification analysis of each of the host proteins over whole cells was carried out on 50 infected and 50 uninfected cells from the same slide, and the arithmetic averages ± SD were calculated using ImageJ software and shown in the graphs. Pearson's coefficients for colocalization of the viral and host proteins in 50 infected cells were calculated and are shown in bar diagrams. Uninf, uninfected cells; Inf, infected cells. Error bars indicate SD.

vary in different cell types, has been reported previously (49, 57–61). Except for DDX6, other DCP body components were observed in both the nucleus and the cytoplasm in serum-grown control cells.

Pan3-positive granules were not observed in the virus-infected or uninfected cells in the same field, and the protein showed a uniform distribution in the cytoplasm and partial relocalization to the nucleus. The protein did not show significant colocalization with the VMs, suggesting that Pan3 dissociated from the DCP granules under serum starvation-induced stress (Fig. 3b). XRN1 appeared to dissociate from the DCP bodies during virus infection and showed partial colocalization with the VMs (Fig. 3b). While DCP1a exhibited increased cytoplasmic relocalization, DCP1b showed enhanced nuclear localization in the infected cells at 8 hpi (Fig. 3b). Both proteins showed partial colocalization with VMs in the virus-infected cells at 8 hpi, as they were primarily distributed uniformly in the cytoplasm due to their dissociation from the DCP granules (Fig. 3b). Some DDX6- and EDC4-positive granules appeared to associate with VMs but dissociated subsequently during the course of infection, resulting in a diffuse distribu-

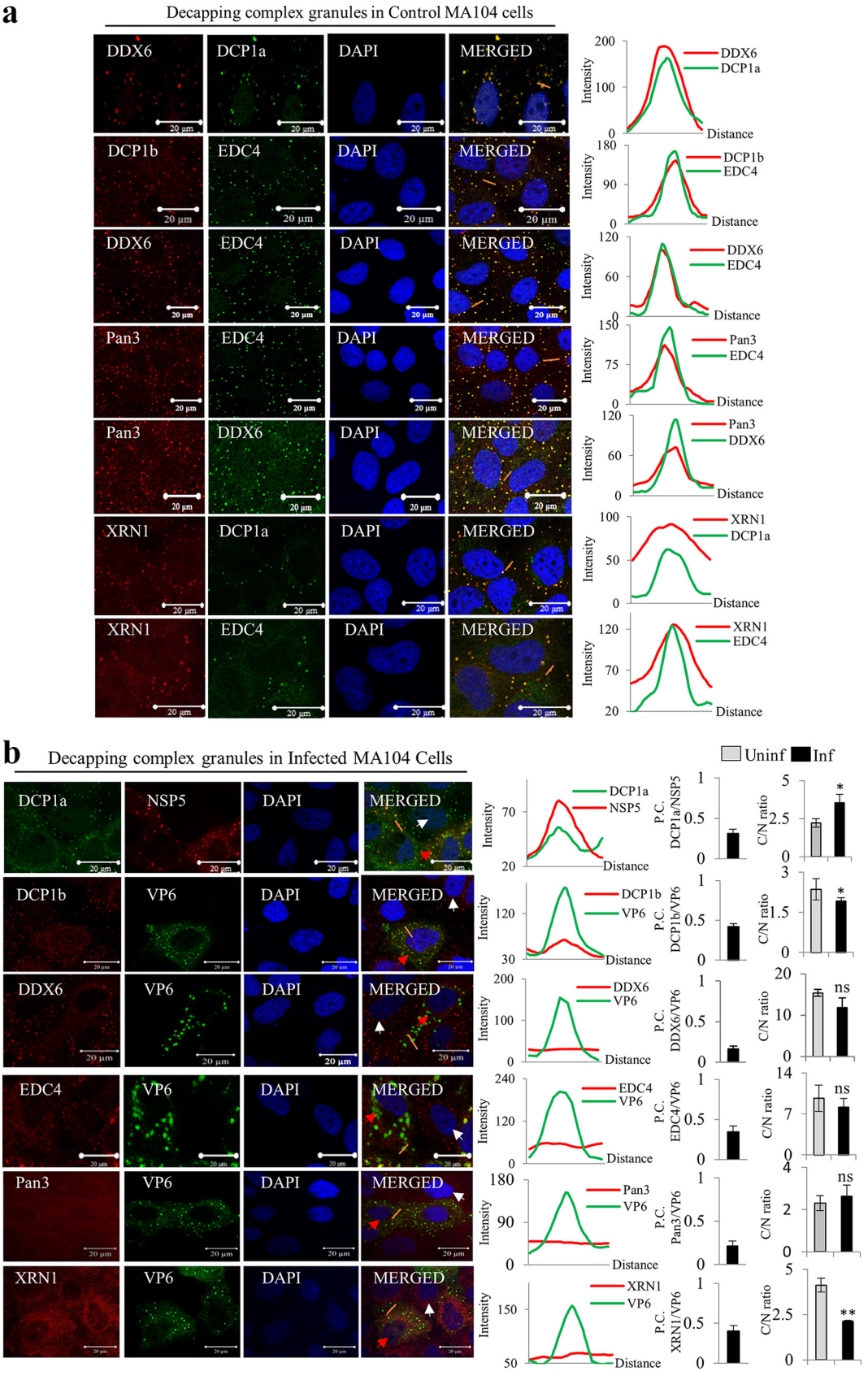

FIG 3 Presence of distinct DCP bodies containing decapping complex proteins in the cytoplasm of serum-grown control cells and their dissociation in virus-infected cells. (a) Colocalization of selected components of the decapping complex in DCP

(Continued on next page)

tion of the proteins in the cytoplasm and a smaller number of the remodeled DCP granules colocalizing with the VMs in the virus-infected cells at 8 hpi (Fig. 3b). The fluorescence quantification of cytoplasmic/nuclear ratios of the proteins in the uninfected and infected cells and Pearson's coefficients of colocalization of the decapping complex proteins with VMs in infected cells are shown in the rightmost panels of Fig. 3b.

Remodeled SG and PB structures colocalize within the same VMs. To investigate if the SG and PB punctate structures/foci represent independent granules or if both coexist in the same foci and colocalize within the same VMs in the virus-infected cells, simultaneous ICM analyses of the viral, SG, and PB proteins for which appropriate antibodies were available were performed using a combination of monoclonal antibodies (MAbs) and PAbs generated in guinea pigs and rabbits. Figure 4 demonstrates that the majority of the SG and PB proteins existed in the same or closely associated granules that colocalized with the same VMs in rotavirus-infected MA104 cells, suggesting sequestration of the large remodeled SG-PB fused structures in the VM.

The colocalization of the ectopically expressed fluorescent protein (FP)-tagged SG and PB proteins YFP-ADAR1, ECFP-Caprin1, mCH-eIF2α, and YFP-DCP1a with the endogenous SG/PB proteins and the virus-expressed viroplasmic proteins in the same VMs at identical positions (Fig. 5a and b) further supports the observation of the colocalization of the endogenous SG and PB proteins/structures with VMs (Fig. 1, 2, 4, and 5).

In contrast to endogenous G3BP1, which neither formed granules nor colocalized with the VM in the infected cells (Fig. 1b), ectopically expressed GFP-G3BP1 induced SGs in the uninfected cells, as reported previously (11, 35), and the GFP-G3BP1-induced foci colocalized with the VMs in the infected cells (Fig. 5b and c). Note that the ectopically expressed YFP-ADAR1, YFP-CPEB, mCH-DCP1a, and ECFP-DDX6 proteins in the uninfected HEK293T cells localized in the cytoplasm and induced the formation of SG/PB punctate structures (Fig. 5c). mCH-eIF2α localized in the cytoplasm. ECFP-hnRNP E1, which was mostly localized to the nucleus, was also present in the cytoplasm but did not induce formation of SG/PB punctate inclusion bodies in the transfected cells. No SG/PB structures were observed in cells expressing ECFP-PKR and ECFP-hnRNP K, as the proteins were primarily localized to the nucleus (Fig. 5c). Note that several RNA-binding proteins expressed in fusion with enhanced cyan fluorescent protein (ECFP), green fluorescent protein (GFP), yellow fluorescent protein (YFP), or mCherry (mCH) exhibited a predominantly nuclear localization in the uninfected transfected cells, as reported recently (11). Further, no SG/PB punctate structures were observed in HEK293T cells ectopically expressing the control ECFP, GFP, and mCH proteins (Fig. 5c). The relative nuclear-cytoplasmic localization and granule-forming properties of the FP-tagged SG/PB proteins are summarized in Table 2.

z-stack analysis of the SG protein ADAR1 and the PB protein GW182 clearly demonstrated the colocalization of the host proteins and the VMs at identical positions (Fig. 6), confirming that the colocalization of the endogenous SG and PB proteins with VMs in the infected cells is not an artifact and is authentic.

Time course ICM analysis of formation of SG and PB punctate structures. Dhillon et al. (11) recently demonstrated that the colocalization of ARE-BPs and hnRNPs

FIG 3 Legend (Continued)
granules in serum-grown control cells. The DCP bodies are negative for GW182-specific PB components. MAbs or PAbs against the decapping complex proteins and Cy3-tagged anti-mouse (green) and Cy5-tagged anti-rabbit (red) IgG secondary antibodies were used. The plot profile path over the DCP granule for colocalization of the two DCP complex proteins is indicated by an orange line. (b) Differential dissociation of the decapping complex proteins during serum starvation-induced stress and RRV infection. Fluorescence quantification of each of the host proteins over 50 infected and 50 uninfected whole cells was carried out using ImageJ software, and the data represent the average C/N ratios over 50 infected and 50 uninfected whole cells from one of three independent experiments and are presented as arithmetic averages $\pm$ standard errors (SE). The plot profile path on the VM for colocalization of the viral and DCP complex proteins is shown by an orange line. Uninfected and infected cells are represented by white and red arrows, respectively. Pearson's coefficients (P.C.) were calculated to assess the colocalization of the viral proteins (NSP5/VP6) with the decapping complex proteins in 50 RRV-infected cells incubated in the absence of serum. Uninf, uninfected cells; Inf, infected cells. The error bars indicate SD. Significance was calculated using Student's *t* test. *, $P < 0.05$; **, $P < 0.01$; ***, $P < 0.001$; ns, not significant.

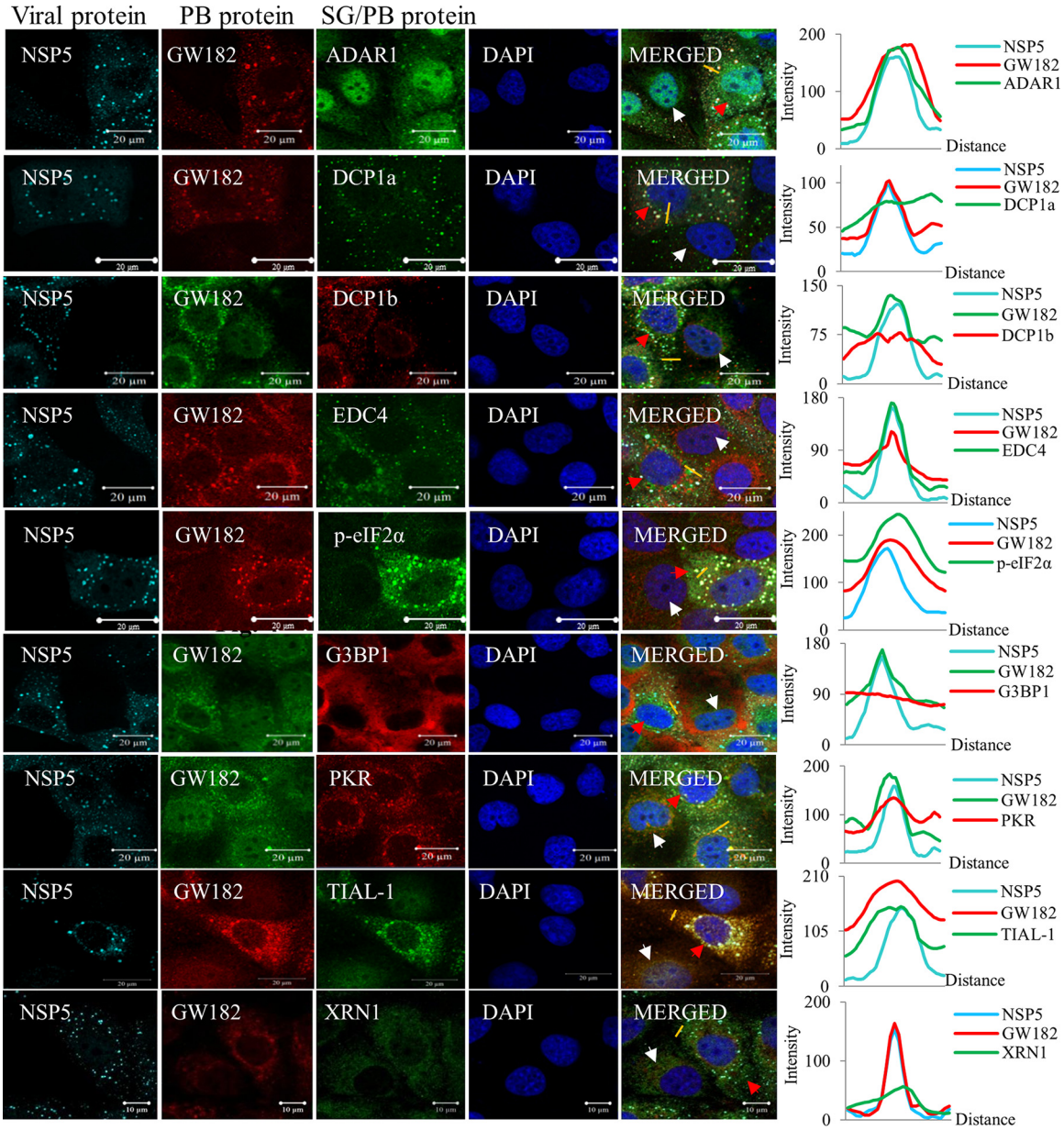

FIG 4 Colocalization of viral viroplasmic proteins and SG and PB proteins in the same inclusion bodies. For colocalization of three different proteins, a guinea pig PAb against NSP5, MAbs or rabbit PAbs against SG and PB proteins, depending on availability, and anti-guinea pig IgG–Alexa Fluor 633, anti-rabbit IgG–Cy5, and anti-mouse IgG–Cy3 conjugate secondary antibodies were used. Uninfected and infected cells are indicated with white and red arrows, respectively. The plot profile path on the VM is indicated by an orange line. The plot profiles of localization of host proteins in the VM are shown in the graphs to the right of the confocal images.

with VMs in rotavirus-infected cells starts at around 4 hpi. From the results in the preceding sections, it is evident that several SG and PB components existed in punctate structures in the cytoplasm at 8 hpi and colocalized with VMs in virus-infected cells (Fig. 1 to 4). To investigate the time of initiation of formation of the remodeled SG and PB granules during the course of virus infection, time course ICM analyses of cells infected with human (KU) and animal (RRV) rotavirus strains were performed. Figure 7a to d reveal the appearance of GW182-positive punctate structures starting at approximately 4 hpi, coinciding with the time of appearance of small VMs, in MA104 cells infected with human (KU) and rhesus (RRV) rotavirus strains. As shown in Fig. 3a and b, DDX6- and EDC4-positive DCP granules existed in the serum-grown and uninfected cells. However, the number of DDX6- and EDC4-positive DCP granules decreased in the infected

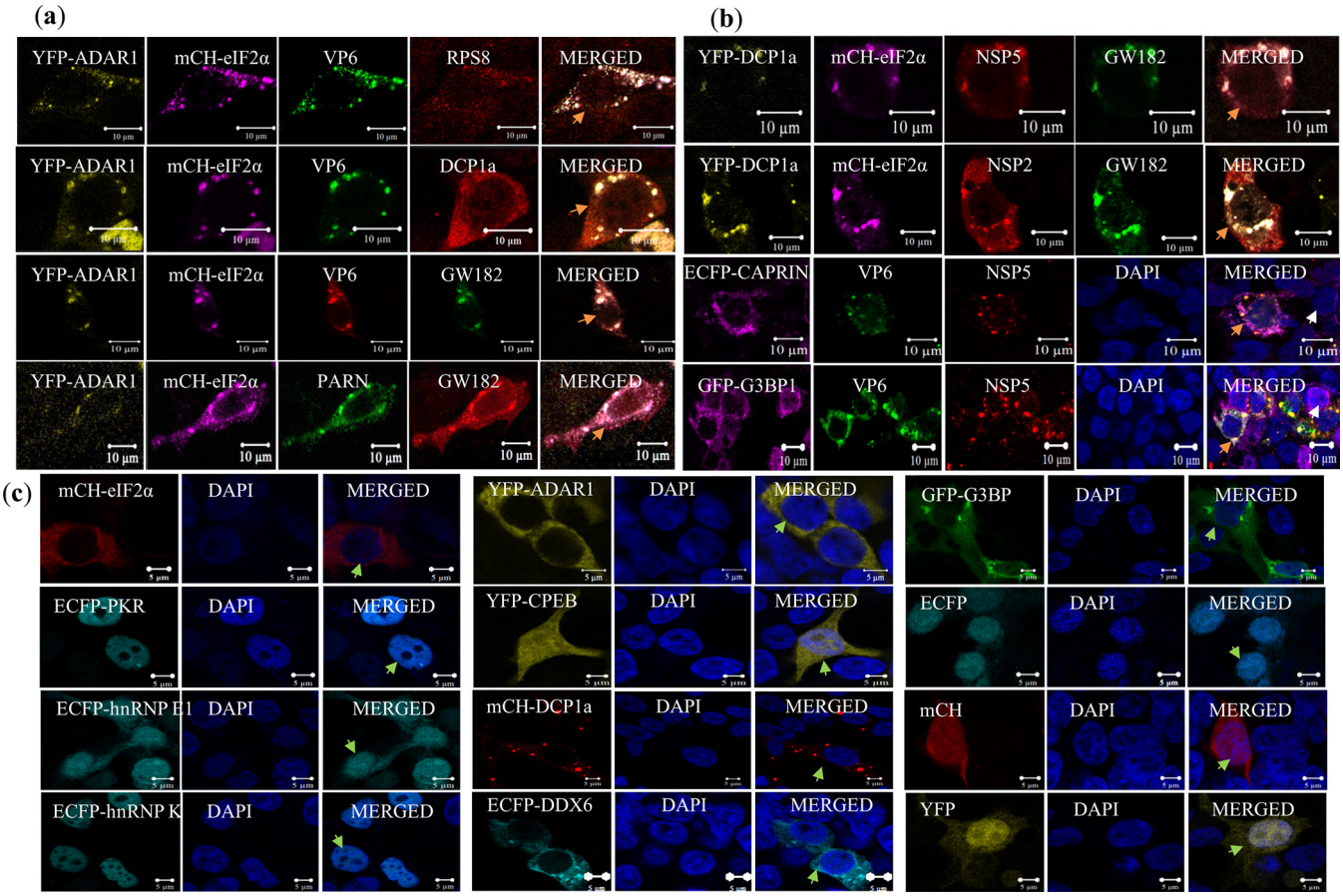

FIG 5 Colocalization of FP-tagged ectopically expressed SG and PB proteins with viral proteins in the VM. (a) Colocalization of ectopically expressed YFP-ADAR1 and mCH-eIF2α with endogenous SG and PB proteins and viroplasmic proteins in the same VMs. HEK293T cells grown on coverslips were cotransfected with plasmid DNA constructs expressing YFP-ADAR1 and mCH-eIF2α for 36 h, followed by RRV infection (0.5 MOI for 8 h). YFP-ADAR1 and mCH-eIF2α were visualized by the protein fluorescence, and the endogenous SG/PB proteins and viral proteins were visualized using Cy3-labeled anti-mouse (green) and Cy5-labeled anti-rabbit (red) IgG secondary antibodies. The transfected-infected cells are indicated with orange arrows. (b) Ectopically expressed YFP-DCP1a, mCH-eIF2α, ECFP-Caprin1, and ECFP-G3BP1 colocalized with endogenous GW182 and viroplasmic proteins in the same inclusion bodies in infected HEK293T cells. Other details are the same as those described for panel a. The induction of formation of SGs by ECFP-Caprin1 and GFP-G3BP1 (pseudocolors) overexpressed in the uninfected cells (white arrows) is clearly seen, while the endogenous G3BP1 is excluded from SGs/PBs/VMs in the infected cells, as shown in Fig. 1, Fig. 3a, and Fig. 4. (c) Granule-forming properties of ectopically expressed fluorescent protein-tagged SG/PB proteins in HEK293T cells. Cells transfected with the expression construct DNA are indicated by light green arrows. No formation of granules in cells transfected with vectors expressing hnRNPs, the control fluorescent proteins, eIF2α, and PKR was observed, but other SG/PB proteins formed foci in the transfected cells. FP-tagged PKR exhibited nuclear localization. Other details are the same as those described for panel a.

cells with the progression of infection in comparison to the number present before infection or in the uninfected cells, as some of the granules exhibited association with followed by dissociation of the proteins from the VMs to assume a uniform diffuse distribution in the cytoplasm between 6 and 8 hpi (Fig. 7). EDC4 dissociation from the granules, in general, was slower than that of DDX6, and some EDC4 granules that were not associated with VMs persisted even after 8 hpi (Fig. 7c and d) but were resolved by 10 hpi.

The existence of the majority of the SG/PB components in punctate structures and their colocalization with each other (Fig. 4) suggest that atypical SGs and PBs containing the majority of their components are formed in infected cells and undergo fusion at approximately 4 hpi. But these structures were negative for the SG marker G3BP1 (Fig. 4 and 7a), which appears to be excluded totally from SG-PB-VM structures despite its high abundance in the cytoplasm (11).

Subcellular dynamics of SG and PB components during the course of rotavirus infection. Dhillon et al. (11) recently demonstrated that rotavirus infection induces cytoplasmic relocalization of several hnRNPs and ARE-BPs. A recent study (71) reported

TABLE 2 Properties of ectopically expressed FP-tagged SG and PB proteins[a]

Protein	Granule formation in transfected cells	Intracellular localization in transfected cells		Localization to VM
		Nucleus	Cytoplasm	
YFP-ADAR1	+	+++	+	+
ECFP-Caprin1	±	±	+++	+
YFP-CPEB	+	+	++	+
mCH-DCP1a	+	+	++	+
ECFP-DDX6	+	−	+++	+
mCH-eIF2α	−	−	+++	+
GFP-G3BP1	+	±	+++	+
ECFP-hnRNPE1	−	+++	+	−
ECFP-hnRNP K	−	+++	−	−
ECFP-PKR	−	+++	±	ND
ECFP	−	++	+	−
YFP	−	++	+	−
mCH	−	++	+	−

[a]The nuclear and cytoplasmic abundances of ectopically expressed FP-tagged proteins are indicated by relative amounts, i.e., −, ±, +, ++, and +++. ND, not determined. YFP, ECFP, and mCH refer to yellow, enhanced cyan, and mCherry fluorescent reporter proteins, respectively.

nuclear relocalization of the PB proteins DCP1a and XRN1 and degradation of Pan3 in virus-infected cells. The ICM analyses discussed in the preceding sections (Fig. 1 to 4) revealed the presence of several SG and PB proteins in both compartments as well as

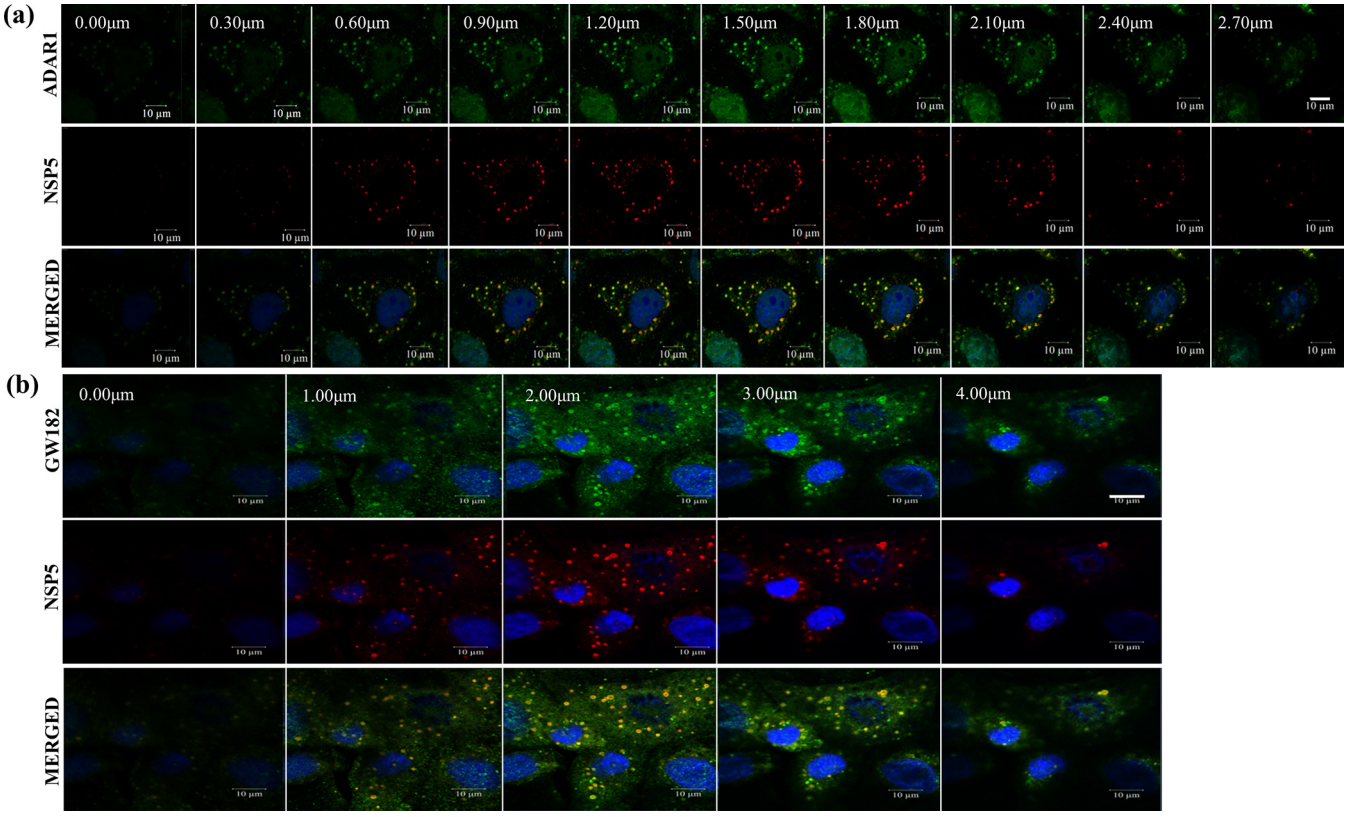

FIG 6 *z*-stack analysis of colocalization of the SG protein ADAR1 and the PB protein GW182 with VMs in RRV-infected MA104 cells. (a and b) Analysis of colocalization of NSP5 with ADAR1 (a) and of NSP5 with GW182 (b) in RRV-infected MA104 cells (at 8 hpi). The proteins were visualized by ICM using rabbit anti-NSP5 and mouse anti-ADAR1 and -GW182 primary antibodies and Cy5-tagged (red) anti-rabbit and Cy3-tagged (green) anti-mouse IgG secondary antibodies. *z*-stacks of images, collected at 0.30-μm intervals ranging from 0 to 2.70 μm for ADAR1 and at 1.00-μm intervals for GW182, using a 4× zoom and a 63× objective under a Zeiss LSM 880 microscope, reveal that both the viral and host proteins were enriched in the same punctate structures in the cytoplasm, suggesting that the colocalization was not due to nonspecific fluorescence or to overlapping diffuse distributions of the two proteins. *z*-stack analyses of other SG and PB proteins also revealed similar results.

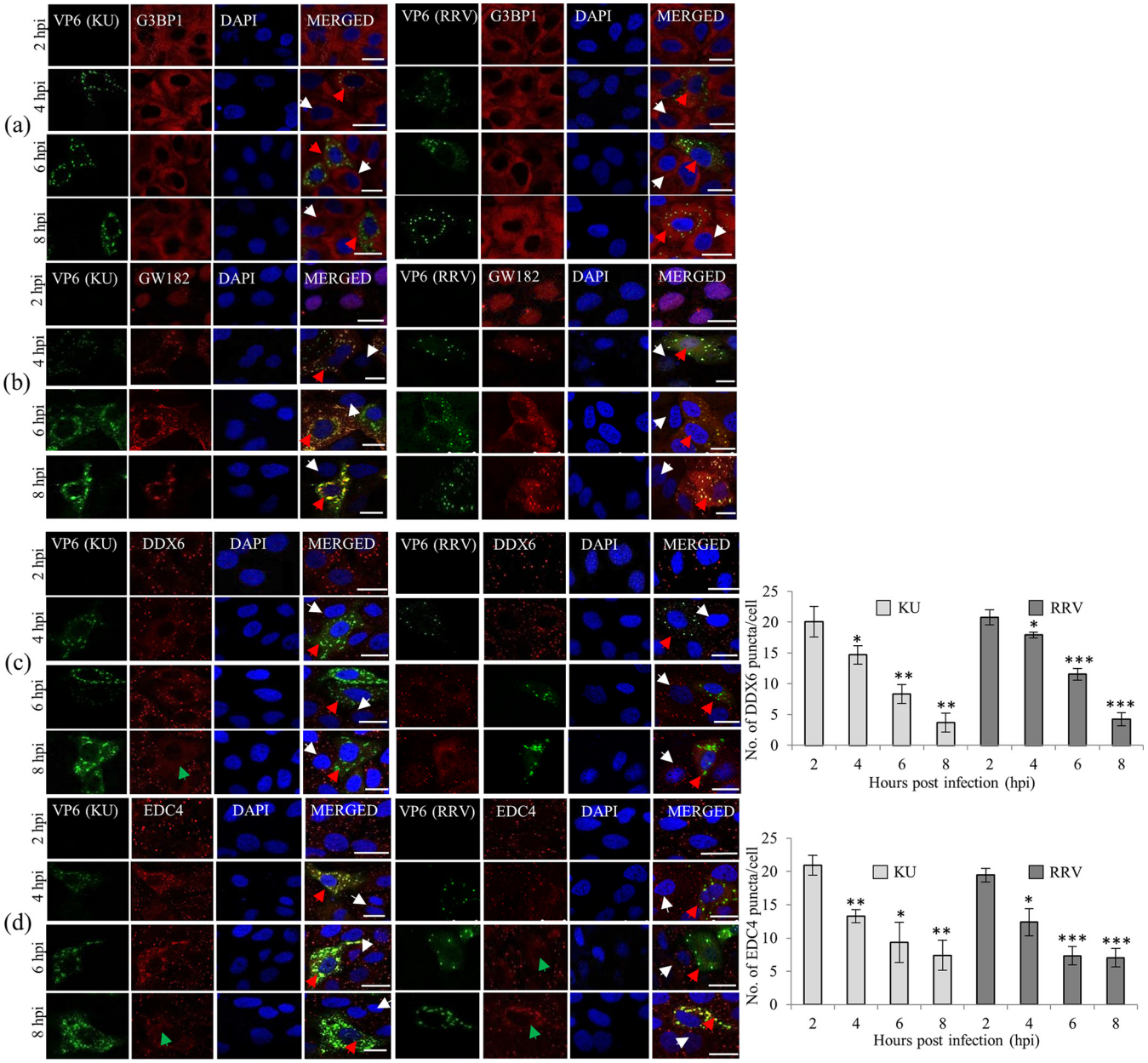

FIG 7 Time course ICM analysis of formation of SG and PB granules in MA104 cells infected with human and animal strains of rotavirus. (a) G3BP1; (b) GW182; (c) DDX6; (d) EDC4. MA104 cells infected with RRV and human rotavirus strain KU were analyzed at 2, 4, 6, and 8 hpi. Both viruses exhibited similar patterns of formation of viroplasms and SG-PB granules. The formation of GW182-positive granules, the appearance of viroplasms, and their colocalization coincided at about 4 hpi. No G3BP1 granules could be detected during the periods of analysis. The colocalization of the PB protein GW182 with VMs and the identical location of the punctate structures of VMs and GW182 at 4 hpi suggest that the colocalization of the host protein with VMs is specific but not due to an abundance of the host protein or to cell lysis. In contrast, not all the DDX6 and EDC4 granules showed colocalization with VMs between 4 and 8 hpi, and the proteins from some of the granules dissociated and attained a diffuse distribution, leading to a reduction in the number of DDX6-EDC4-positive granules at late time points of infection. Uninfected and virus-infected cells are indicated by white and red arrows, respectively. Infected cells in which DDX6 and EDC4 granules underwent dissociation followed by diffuse distribution of the proteins between 6 and 8 hpi are indicated by dark green arrows. The arithmetic averages ± SD of the numbers of DDX6 and EDC4 granules per KU- or RRV-infected cell at 2, 4, 6, and 8 hpi were calculated using ImageJ software and are presented in the bar diagrams. The existence of decapping complex proteins in granules in the cytoplasm of serum-grown control cells is described in the legend to Fig. 3. Bars, 20 μm.

relocalization (of DCP1a, DCP1b, Pan3, and XRN1) during virus infection (Fig. 1a and b, Fig. 2, Fig. 3b, and Fig. 4).

To clearly understand the dynamics and intracellular localization of SG and PB proteins during rotavirus infection, a large number of them were examined by WB analysis of the nuclear and cytoplasmic fractions from serum-grown control, mock-

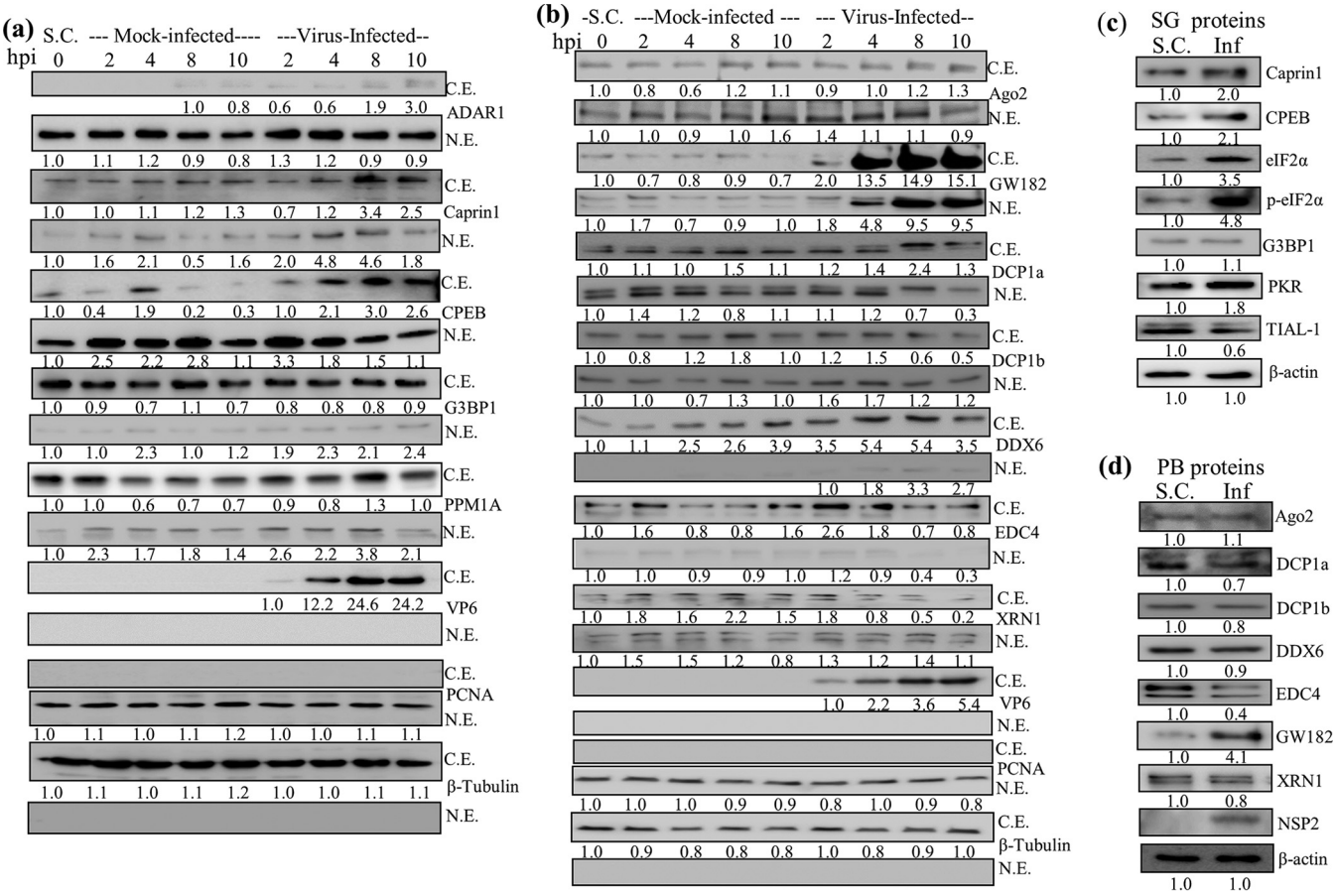

FIG 8 Analysis of nuclear and cytoplasmic distribution of SG and PB components in mock-infected and RRV-infected MA104 cells during the course of infection. (a) Time course immunoblot analysis of the levels of SG proteins in the nuclear and cytoplasmic fractions. The samples in lane 0 (hpi) represent nuclear and cytoplasmic fractions from serum-grown control cells. Lanes for 2 to 10 hpi in the left half of the panel represent mock-infected cells incubated for the indicated periods in medium lacking serum, identical to the conditions under which virus infections were done. Lanes for 2 to 10 hpi in the right half of the panel represent extracts prepared from RRV-infected cells. VP6 was detected using subgroup I MAb 631/9, which is specific to the viral protein, with no cross-reactivity to host proteins. β-Tubulin and PCNA were used to determine the purity of the cytoplasmic and nuclear fractions, respectively, and as internal loading controls. Fifty micrograms of protein was analyzed at each time point. hpi, hours postinfection; C.E., cytoplasmic extract; N.E., nuclear extract. The fold changes in the levels of the proteins in the mock-infected and virus-infected cells in comparison to those in the serum-grown control cells (0 hpi) are given at the bottom of each blot. If a protein was undetectable in the serum-grown control cells (S.C.), the time point at which it was first detectable in the respective compartment was taken as the reference for fold change calculations (11). (b) Analysis of the altered nuclear and cytoplasmic distribution of PB proteins during rotavirus infection. Details of the analysis are the same as those described for panel a. The absence of bands corresponding to PCNA and ADAR1 in the cytoplasmic fractions and of those for β-tubulin and VP6 in the nuclear fractions from the serum-grown control, mock-infected, and virus-infected cells when 50 μl of protein was analyzed indicates the purity of the respective preparations (11). (c and d) Analysis of the total protein levels of SG proteins (c) and PB proteins (d) in control and virus-infected cells. The fold changes in the levels of the proteins in the infected cells at 8 hpi, shown at the bottom of each blot, were calculated with reference to the levels in the serum-grown control cells (S.C.).

infected, and virus-infected MA104 cells. For convenience, the proteins are discussed according to their intracellular localization patterns. ADAR1 (Fig. 8a) was localized primarily in the nucleus in the serum-grown control cells and showed partial relocalization to the cytoplasm in mock-infected, uninfected, and virus-infected cells. CPEB was also localized predominantly in the nucleus, but it was also detectable in the cytoplasm. Both proteins showed increased cytoplasmic relocalization with progression of infection (Fig. 8a). While no significant change in the nuclear level of ADAR1 was observed, that of CPEB decreased during late infection. In contrast, DDX6 (Fig. 8b) was primarily a cytoplasmic protein in serum-grown control and mock-infected MA104 cells but exhibited partial relocalization to the nucleus during virus infection. The level of DDX6 in the cytoplasm increased in response to serum starvation-induced stress in the mock-infected cells, and this was further enhanced during virus infection. EDC4 was predominantly cytoplasmic, with a low level of the protein detectable in the nucleus, but it showed decreased levels in both compartments at 8 hpi in the virus-infected

cells. The Mg^{2+}/Mn^{2+}-dependent Ser/Thr phosphatase PPM1A, which negatively regulates stress response pathways, was predominantly cytoplasmic but was also constitutively present in the nucleus, and its level in the cytoplasm increased during later stages of virus infection (Fig. 8a). Caprin1 (Fig. 8a) was present at significant levels in both compartments in the control, mock-infected, and virus-infected cells. While the levels of Caprin1 increased in the nucleus in response to serum starvation-induced stress, it exhibited increased cytoplasmic accumulation with progression of infection, with a concomitant decrease in its nuclear levels. G3BP1 was predominantly cytoplasmic but was also detectable in the nuclear fractions in the serum control, mock-infected, and virus-infected cells. No significant change in the level of G3BP1 in the cytoplasm under different conditions was observed, but there was a small increase in the nucleus in the mock- and virus-infected cells. Interestingly, the levels of GW182 (TNRC6), a major PB component, increased in the cytoplasm of mock-infected cells without a significant change in the nuclear level, but its levels were greatly enhanced in both compartments during virus infection (Fig. 8b). The level of Ago2 in the cytoplasm increased in response to serum starvation-induced stress, but no significant change in its level was noticed in the nucleus or cytoplasm during virus infection (Fig. 8b).

Note that DCP1a and DCP1b were present in both compartments in serum control and mock-infected MA104 cells but showed contrasting intracellular relocalization during virus infection. While DCP1a showed increased cytoplasmic accumulation with a concomitant decrease in the nucleus during late times of virus infection, DCP1b exhibited increased nuclear accumulation with a concomitant decrease in the cytoplasm (Fig. 8b). XRN1 was also present in both compartments but showed nuclear relocalization during virus infection (Fig. 8b). The results obtained by WB analyses of the nuclear and cytoplasmic fractions closely corresponded with those observed for ICM analyses (Fig. 1 to 3). The relative changes in the levels of the SG and PB proteins during virus infection and mock infection compared to the levels in the serum-grown control cells are shown at the bottom of the WB for each protein (Fig. 8a and b). Tables 1 and 2 summarize the relative localization and abundance levels of different proteins in the infected cells at 8 hpi compared to those in the serum-grown control cells. The relative changes in the nuclear and cytoplasmic levels of different proteins in the infected cells at 8 hpi with reference to those in the serum-grown control cells (Fig. 8a and b) closely correlated with the total protein levels in the infected cells at 8 hpi (Fig. 8c and d).

Interaction of SG and PB components with viroplasmic proteins NSP2 and NSP5. Recently, many ARE-BPs and hnRNPs and some cytoplasmic proteins were shown to interact directly with NSP2 and/or NSP5 and to colocalize with the VMs in virus-infected cells (11). Since SG and PB proteins also showed colocalization with the VMs, their possible interaction with the viroplasmic proteins NSP2 and NSP5 was examined by a pulldown (PD) assay using RNase-treated and untreated control cell extracts and recombinant proteins to understand the possible molecular basis for their sequestration in the VM. Note that infected cell extracts were deliberately not used in the PD assays, as it would not be possible to understand whether the SG/PB protein was directly interacting with the bead-bound viral protein or was indirectly recruited through its interaction with other viral or host proteins present in different SG, PB, and viroplasmic complexes, as recently described by Dhillon et al. (11). Figure 9a demonstrates that the majority of the SG and PB proteins interacted with NSP2 and/or NSP5 in an RNA-independent manner. Note that the PB protein Pan3 did not bind to either NSP5 or NSP2. Caf1-p150 showed RNA-dependent binding to NSP2 but not to NSP5. The eIF2α interaction with NSP2 was RNA independent, but that with NSP5 was RNA dependent. In contrast, PKR showed RNA-independent binding to NSP5 but no binding to NSP2. Ago2 and Caprin1 bound to NSP5 in an RNA-independent manner and also showed RNA-dependent binding to NSP2. The other SG and PB proteins that were examined exhibited RNA-independent binding to both NSP2 and NSP5. The observation that the majority of the SG and PB components directly interacted with NSP2 and/or NSP5 was further confirmed by a direct-binding PD assay (Fig. 9b and c) using

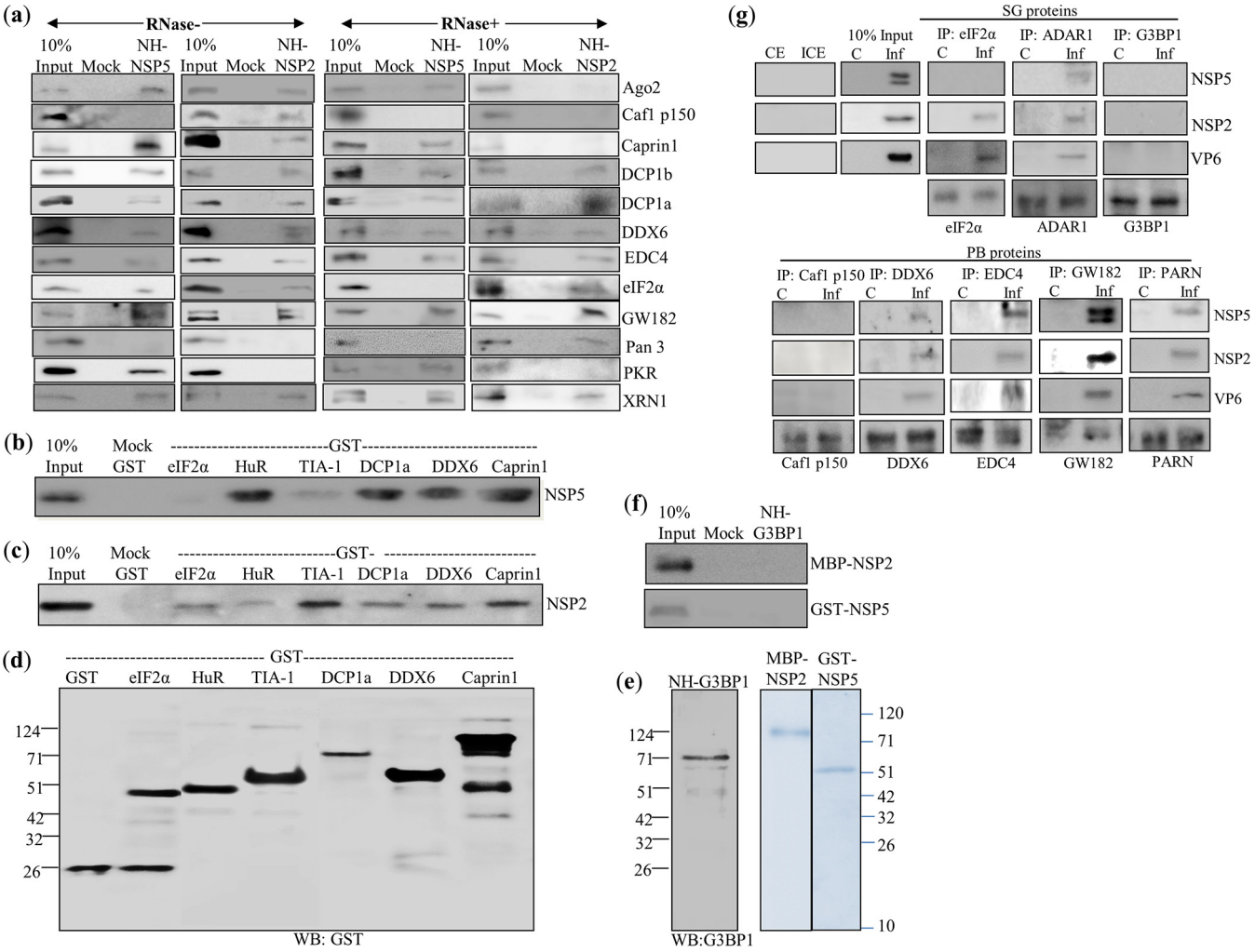

FIG 9 Demonstration of interaction of host SG and PB proteins with viroplasmic proteins by pulldown (PD) assays and coimmunoprecipitation (co-IP) analyses. (a) Analysis of interactions between recombinant viral NSP2 and NSP5 and host SG and PB proteins. The NH-tagged NSP5 and NSP2 proteins were purified from *E. coli* by affinity chromatography using Ni^{2+}-nitrilotriacetic acid (NTA)-agarose beads. Control Ni^{2+}-NTA-agarose beads used for mock binding were prepared by incubation with a lysate of *E. coli* harboring the pET22-NH vector lacking the viral gene. Both the control and viral protein-bound beads were further saturated by storage at 4°C in 0.5% bovine serum albumin (BSA) to minimize nonspecific binding of cellular proteins. The RNase-treated purified recombinant NSP2 and NSP5 proteins bound to Ni^{2+}-NTA-agarose beads and the control beads (mock binding) were incubated with equal amounts (500 μg) of cell extracts, prepared from serum-grown control MA104 cells, that were either treated or not treated with RNase A as indicated above the panels. The cellular proteins bound to the beads were resolved by SDS-PAGE, and the interacting SG and PB proteins were detected by immunoblotting as described recently (11). In the lane representing 10% input, 50 μg of RNase-treated or untreated cell extract was used. The same blot was used to detect two host proteins by sequential deprobing and reprobing, depending on clear differences in their molecular weights to confirm the presence of more than one protein in the protein complex, as described previously (11). Each PD assay was repeated 3 or 4 times to confirm reproducibility. RNase treatment of cell extracts and other details were described recently (11). (b and c) Demonstration of direct interactions between purified NH-NSP2 and NH-NSP5 and glutathione bead-bound, GST-tagged SG and PB proteins. Ten micrograms of purified NH-NSP2 or NH-NSP5 was incubated with approximately 2 μg of bead-bound recombinant GST-tagged eIF2α, HuR, TIA1, DCP1a, DDX6, or Caprin1 treated with RNase A (10 mg/ml), and the bound viral protein was detected by Western blotting using specific antibodies against NSP2 and NSP5. Direct binding assays using GST-PKR and GST-Caf1-p60 were not performed, as the full-length proteins could not be purified due to their cleavage into several fragments when expressed in *E. coli*. (d and e) Expression and purification of GST-tagged recombinant SG and PB proteins (d) and of NH-G3BP1, maltose-binding protein (MBP)-tagged NSP2, and GST-tagged NSP5 (e). The bacterial cell extracts were incubated with RNase A (100 mg/ml) for 45 min at room temperature prior to purification of the proteins. The purified proteins were resolved by SDS-PAGE and detected by staining with Coomassie blue R250. (f) G3BP1 does not bind to NSP2 or NSP5. Eluted MBP-NSP2 and GST-NSP5 were incubated with bead-bound NH-G3BP1, and bound NSP2 and NSP5 were detected using specific antibodies. (g) Demonstration of association of SG and PB proteins with viroplasmic complexes in infected cells by co-IP analyses. Immune complexes with SG and PB proteins and protein-specific antibodies were captured with BSA-saturated protein A-agarose beads, and the viral proteins in the complexes were detected by WB. CE and ICE represent control co-IPs performed using control cell extract and infected cell extract, respectively, demonstrating that the detection of viral proteins in the co-IPs is specific.

RNase-treated purified N-His (NH)-, glutathione *S*-transferase (GST)-, or maltose-binding protein (MBP)-tagged recombinant viroplasmic proteins and selected NH- or GST-tagged SG and PB proteins (Fig. 9d). Purified NH-G3BP1 (Fig. 9e) failed to bind to purified NSP2 or NSP5 (Fig. 9e and f).

The association of SG and PB components with the VMs or subviroplasmic complexes in the infected cells was further examined by coimmunoprecipitation (co-IP) analyses using RNase-treated infected cell lysates. With the exception of G3BP1 and Caf1-p150, antibodies against other SG/PB proteins coimmunoprecipitated the viral proteins NSP2, NSP5, and/or VP6 (Fig. 9g). Note that the viral proteins were undetectable in the co-IP complexes of G3BP1, which neither interacted with NSP2 or NSP5 in the PD assay nor colocalized with the VM (Fig. 1a and 9a). The observation that Caf1-p150 bound only to NSP2 in an RNA-dependent manner and was undetectable in the co-IP complexes from RNase-treated cell extracts suggests a loss of its association with VMs upon RNase treatment. The interactions between the SG/PB proteins and the viroplasmic proteins NSP2 and NSP5 and their colocalization with the VM are summarized in Table 1.

Biological significance of SG and PB components for viral protein expression and rotavirus growth. The biological significance of the nuclear-cytoplasmic dynamics of the SG and PB proteins and colocalization of the remodeled SGs and PBs with VMs or diffuse distribution of some of their components in the cytoplasm was assessed by small interfering RNA (siRNA)-mediated downregulation of expression and/or ectopic overexpression of selected proteins. Analysis of the influence of some of the SG and PB proteins on the levels of expression of the viroplasmic proteins NSP2, NSP5, and VP6 revealed that, except for ADAR1, the majority of the proteins that were examined negatively affected the expression of all three viral proteins (Fig. 10a to c). Figure 10d represents the quantification of the levels of individual viroplasmic proteins from three independent experiments. The positive or negative influence of the SG and PB proteins on virus infection was further examined by determining the infectious virus yield in HEK293T cells transfected with siRNA or an expression plasmid construct followed by virus infection. Figure 11 demonstrates that siRNA-mediated downregulation of expression of the majority of the SG and PB proteins significantly enhanced the infectious progeny virus yield, by 1.2 to 2.2 orders of magnitude. Since EDC4 and DDX6 are associated with scaffolding and helicase activities but not directly associated with decapping activity, the effect of downregulation of expression of these two DCP body proteins appeared to be significantly less than that observed when DCP1a was downregulated. Further, the free EDC4-positive granules that were not associated with VMs were two times more abundant than the DCP1-positive free granules in the infected cells at 8 hpi (Fig. 3b), suggesting that downregulation of expression of EDC4 or DDX6 and DCP1 may have differential effects on viral protein expression and the progeny virus yield. Ectopic expression of G3BP1 and Caprin1 inhibited virus growth to similar extents. G3BP1 appears to be a potent negative regulator of rotavirus infection. Rotavirus infection appears to inhibit the formation of G3BP1-positive normal functional SGs by selective exclusion of G3BP1, which is a critical SG nucleating component. Although the precise underlying principle for exclusion of G3BP1 from SGs is not understood, rotavirus appears to inhibit normal stress granule formation so that their normal functions are altered or modulated to promote viral protein synthesis under the stress conditions of virus infection. While the activities of the host proteins can be modulated by sequestration in the VM, exclusion of G3BP1 from the SGs and VMs also appears to serve the same function. Overexpression of G3BP1 is known to drive formation of SGs (11, 35). Our demonstration of the negative influence of G3BP1 on viral protein expression and progeny virus production when it is ectopically overexpressed (Fig. 10c and d and Fig. 11) further suggests that G3BP1-driven SG formation is detrimental for productive rotavirus infection despite the lack of its direct interaction with the viroplasmic proteins. The phosphatase PPM1A also had a negative effect on virus growth. Among the SG/PB proteins that were investigated, only ADAR1 exhibited a positive effect on the infectious virus yield (Fig. 11).

DISCUSSION

The present study, involving analysis of a large number of SG-PB components, demonstrated that rotavirus induces formation and sequestration in the VMs of atyp-

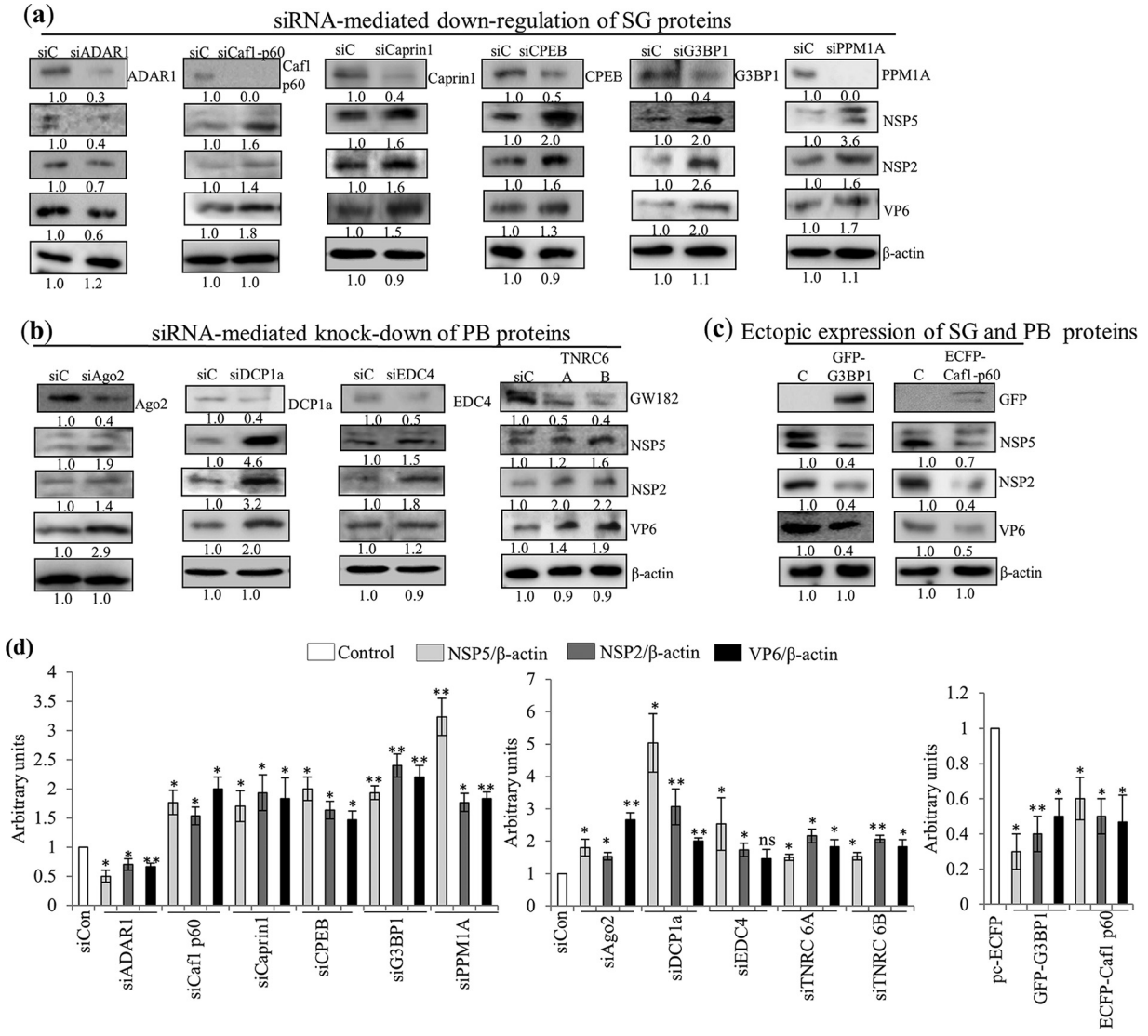

FIG 10 Effects of siRNA-mediated knockdown and ectopic expression of SG and PB proteins on viral protein expression. (a) Western blot analysis of effects of siRNA-mediated downregulation of expression and ectopic expression of SG proteins on viroplasmic protein expression. HEK293T cells were transfected with 30 pmol of siRNA against the host protein for 48 h, followed by infection with purified RRV at an MOI of 5. At 8 hpi, cell extracts were prepared, and 50 μg of total protein was used for detection of NSP2 and NSP5 by use of PAbs and of VP6 by use of MAb 631/9 in WB as described by Dhillon et al. (11). Control cells were transfected with Accell nontarget siRNA as a negative control. (b) Analysis of the effect of siRNA-mediated downregulation of expression of PB proteins on viral protein expression. (c) Effect of ectopic expression of SG and PB proteins on viroplasmic protein expression. HEK293T cells were transfected with plasmid DNA (0.75 μg/well) expressing GFP-G3BP1 or ECFP-Caf1-p60 for 48 h, followed by infection with purified RRV at an MOI of 5. Viral proteins were analyzed at 8 hpi. (d) Quantification of expression levels of viral proteins in virus-infected cells in which the expression of SG/PB proteins was downregulated or overexpressed. The fold changes in protein levels in the siRNA-transfected virus-infected cells in comparison to those in serum-grown control cells transfected with control siRNA were calculated from three independent experiments and are presented in the bar diagrams as means ± SD. While enhanced expression of all three viroplasmic proteins upon knockdown of expression of the selected SG/PB proteins was observed, knockdown of ADAR1 resulted in reduced levels of expression of the viral proteins. Ectopic expression of G3BP1 and Caf1-p60 reduced the level of viral protein expression in comparison to that in cells transfected with the control plasmid pECFP. Expression of the control GFP and ECFP proteins had no significant effect on viral protein expression. Statistical analysis was done using Student's *t* test, and the significance of the results is as described in the legend to Fig. 1.

ical/remodeled SGs and PBs containing the majority of their components, with selective exclusion of a few proteins. This finding is in contrast to previous observations based on the lack of detection of a few SG and PB components in punctate structures in rotavirus-infected cells (11, 70, 71).

In a previous study, Bhowmick et al. (71) reported disruption of PBs in rotavirus-infected cells based on the analysis of only three decapping complex proteins, DCP1a, XRN1, and Pan3, in the absence of knowledge on the status of the large number of

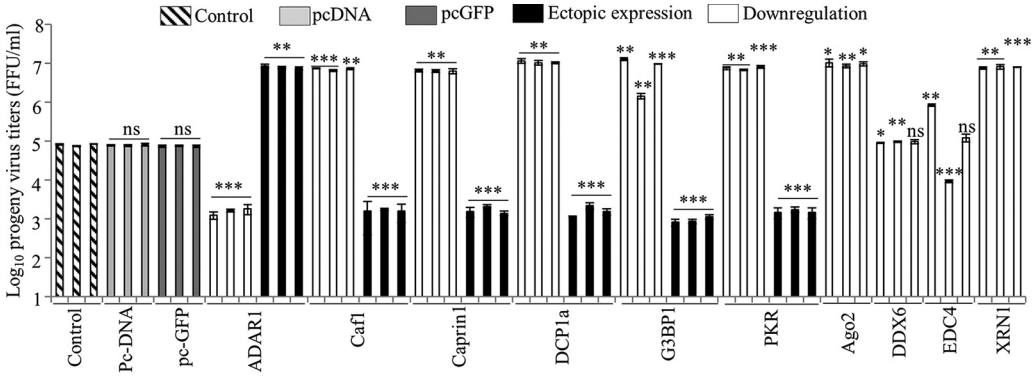

FIG 11 Effect of siRNA-mediated knockdown and/or ectopic expression of selected SG/PB proteins on progeny virus yield. HEK293T cells in duplicate wells in a 24-well plate were transfected with siRNAs against the SG and PB proteins or with the ECFP-, GFP-, YFP-, or mCH-tagged SG/PB protein expression constructs for 48 h as described in the legend to Fig. 10, followed by infection with 400 FFU of purified RRV. Nontarget fluorescent Accell siRNA was used as a control. At 8 hpi, cell lysates were prepared in DMEM by the freeze-thaw method. For progeny virus titer determination, confluent MA104 cells were infected with serial dilutions of lysates from transfected-infected HEK293T cells, and the progeny virus titers in two wells each from three independent experiments were determined by ELIFA as described in Materials and Methods. VP6 MAb was used for detection of infected cells, and the deep brown foci were counted under a microscope (11, 132). The progeny virus yields per milliliter from three different experiments were plotted independently. For control infections, untransfected control HEK293T cells and cells transfected with either pc-DNA 3.0 or pc-GFP expression vectors were used.

other PB components. The present study clearly demonstrates the existence of a large number of granules, called DCP bodies (consisting of decapping complex proteins) (49, 53, 56, 58–61), which are negative for other SG and PB markers, such as G3BP1, GW182, and Caprin1, in serum-grown control cells (Fig. 3a and b). Rotavirus infection appears to induce destabilization of the DCP bodies by differential dissociation and intracellular relocalization of the components of the decapping complex. In contrast to the previous report (71), our studies involving nuclear-cytoplasmic relocalization and ICM analyses demonstrate that DCP1a accumulates in the cytoplasm and shows partial colocalization with VMs, besides being present in diffuse form, in infected cells. The transient association of DDX6- and EDC4-positive DCP granules with VMs and their subsequent dissociation from the VMs, resulting in diffuse distribution and reduction in the number of DCP granules with progression of infection, are interesting. Some EDC4-positive granules could be seen for a longer period than those positive for DDX6 (Fig. 7c and d), probably due to the scaffolding function of EDC4 in the granules (58). Association of the functional decapping complex with the mRNA decay activators hUPF1 and TTP enhances decapping of the target AU-rich mRNAs (45, 46). In this context, with rotaviral mRNAs being 57% to 68% AU rich (11), destabilization of the decapping machinery in the cytoplasm appears to be an important viral strategy for promoting productive virus infection.

In contrast to the presence of the decapping complex proteins in granules in the cytoplasm in the serum-grown control cells, other SG and PB proteins primarily existed in a dispersed state in the nucleus and/or cytoplasm in control and mock-infected cells (Fig. 1a and b, Fig. 2, and Fig. 3a and b), suggesting that rotavirus infection induces molecular triage and remodeling of the SGs and PBs by selective exclusion of the key SG marker G3BP1 and of ZBP1 (Fig. 1b). While the decapping complexes in the PBs were subjected to destabilization by differential dissociation of the components, leading to partial colocalization with the VMs during rotavirus infection, the majority of the SG and PB components existed in granules in rotavirus-infected cells and colocalized with the VMs until the end of the virus life cycle. It is significant that the appearance of the remodeled SG and PB granules coincided with that of the VMs in the virus-infected cells at 4 hpi (Fig. 7). Co-IP analyses of selected proteins by use of infected cell lysates (Fig. 9g), the direct interaction of SG and PB proteins with the viroplasmic proteins (Fig. 9b and c), and the colocalization with VMs of the ectopically expressed fluorescent protein-tagged SG/PB proteins (Fig. 5) further confirmed the association of SG/PB components with the VMs.

Different viruses modulate the composition of SGs and PBs, inhibit or promote their formation, or hijack or inactivate a few specific components of these bodies to promote productive virus infection (29, 42, 47, 50, 61, 67–69, 72–80). However, rotavirus appears to employ sequestration of the large remodeled SG and PB granules in the VM, selectively excluding a few of their components, as a novel strategy to promote virus replication. siRNA-mediated knockdown and ectopic expression analyses of selected SG/PB proteins revealed that the majority of the SG and PB proteins, including those of the decapping complex, negatively influence virus growth. Only ADAR1, which is present in the nucleus and the cytoplasm in infected cells and is also localized in the VM (Fig. 1a and Fig. 4), promoted the infectious progeny virus yield (Fig. 11). Previous studies reported a positive influence of ADAR1 on the growth of other viruses by inhibition of PKR activity and SG formation (81–83). Interestingly, the phosphatase PPM1A, which negatively regulates host stress response pathways and antiviral defense mechanisms (84, 85), is upregulated and is also localized to the VM in rotavirus-infected cells. The enhanced viral protein expression and progeny virus yield in cells in which PPM1A protein expression is downregulated by siRNA suggest that its phosphatase activity is detrimental to virus growth (86). The PP2C family phosphatases play important roles in several cellular processes, including nuclear transport, and their activities are regulated by posttranslational modifications, such as phosphorylation and N-myristoylation (87–90). It is of interest to investigate the mechanism(s) by which the phosphatase activity is regulated in rotavirus-infected cells to promote virus growth (86).

It could be argued that the interactions between the recombinant viral proteins and the host proteins in the *in vitro* PD assays are nonspecific due to the improper folding of the recombinant proteins and lack of posttranslational modifications that occur in proteins expressed in mammalian cells. Although the *in vitro* interactions between the viral proteins and the SG and PB proteins appear to be RNA independent, it is likely that RNA-mediated interactions play a very important role in the assembly of the complex supramolecular rotavirus replication organelles inside the infected cell, since the majority of the SG and PB proteins as well as NSP2 and NSP5 are RNA-binding proteins. Further, it is unlikely that a single NSP2 or NSP5 molecule simultaneously interacts with several host proteins. Since VMs contain a large number of NSP2 and NSP5 molecules, it is likely that individual NSP2 and NSP5 molecules interact with one or two different host proteins. The fact that the majority of the SG and PB proteins and other host proteins (11) are associated with viral proteins in the VMs inside the cell, as revealed by ICM analyses and co-IP analyses using infected cell extracts, renders irrelevant the argument that the interactions between viral and host proteins in the *in vitro* PD assays are nonspecific.

It is intriguing that the viroplasmic proteins NSP2 and/or NSP5 showed interaction with a large number of host hnRNPs, ARE-BPs, cytoplasmic proteins (11), and SG and PB components that are associated with VMs. It is tempting to speculate that the mechanism of assembly of the VM and its association with a plethora of host proteins are analogous to the assembly of SGs and PBs. Many proteins of SGs and PBs contain intrinsically disordered regions (IDRs), low-complexity domains (LCDs), or prion-like domains (30, 91–95), which promote liquid-liquid phase separation via multivalent weak protein-protein, RNA-protein, and RNA-RNA interactions (96, 97), causing liquid demixing, formation of phase-separated liquid droplets, and reversible aggregation of the translationally stalled preinitiation mRNP complexes (30, 91–97). The transient association with and dissociation from the VMs of the decapping complex components likely reflect the dynamic nature of interaction of some of the host proteins with the VMs. In this context, the N-terminal half of NSP5 was reported to be a low-sequence-complexity and disordered/unstructured region and the C-terminal region to be a helical region, which is required for decamerization of the protein, interaction with other viral proteins, and VM formation (98–102). Both the N- and C-terminal regions of NSP5 were reported to interact with NSP2 (9, 23, 100). NSP2 binding induces hyperphosphorylation of NSP5, which is required for mature VM formation (100, 102).

Turning next to NSP2, the C-terminal helical tail (CTH) was reported to assume a phosphorylation-dependent open conformation that is important for mature VM formation and its interaction with viral and cellular proteins, such as tubulin (103–107). Based on these observations, it is tempting to speculate that the N- and C-terminal regions in NSP5 and the CTH in NSP2 are important not only for the assembly of viroplasmic proteins in the VM but also for the sequestration of host proteins by weak protein-protein and RNA-protein interactions, but these speculations require detailed investigations.

Protein phosphorylation, methylation, acetylation, glycosylation, and PARylation affect assembly and disassembly of SGs and PBs, suggesting a potential link between signal transduction and mRNA stability (30, 37, 91, 108–116). Many host RNA-binding proteins also undergo posttranslational modifications, such as phosphorylation, methylation, acetylation, and SUMOylation, in response to environmental stimuli, stress, and virus infection, which influence their functions associated with nuclear-cytoplasmic localization, RNA binding, protein-protein interactions, and RNA metabolism (117–123). The viral viroplasmic proteins are also known to undergo phosphorylation, glycosylation, methylation, and/or SUMOylation in virus-infected cells (98–100, 102, 106, 124–127). The events leading to the assembly of mature VMs are modulated by phosphorylation of NSP2 and NSP5 (106). The roles of other posttranslational modifications in the viroplasmic proteins in VM formation need to be investigated. Since several signaling pathways are activated in rotavirus-infected cells (128–131), it is important to investigate the role of posttranslational modifications in the interactions between the viral proteins and host proteins leading to the sequestration of the host proteins in the VM during virus infection.

The finding that rotavirus sequesters the complex SG-PB cellular organelles that are associated with translational suppression and mRNA degradation in the VM is quite unexpected. The coexistence of the majority of the components of SGs and PBs with the VM through the virus life cycle suggests that the translationally stalled host mRNAs are destined for degradation and are not released further for translation. By hitchhiking in the host mRNA degradation organelles, the virus may derive benefit by harnessing their RNA degradation property to channel a continuous and rapid supply of nucleotides from the degraded cellular RNAs to the viral genome replication machinery for efficient replication of the viral genome within the short period of the virus life cycle. However, the nucleoside monophosphates (NMPs) generated from degradation of host mRNAs in the SG-PB complexes have to be converted into nucleoside diphosphates (NDPs), which may then serve as substrates for NSP2 for their conversion into nucleoside triphosphates (NTPs) directly in the VM by its NDP kinase activity (132). Our unpublished observation of sequestration of host NMP kinases, as well as that of NDP kinase (nm23) (133, 134), in the VM appears to support this hypothesis. Moreover, by sequestration of the remodeled SGs and PBs in the VM and dissociation of DCP bodies, the virus appears to inhibit/seclude them from accessing the translating viral mRNAs in the cytosol and protect them from translational repression and mRNA degradation. The coincidence of the time of appearance of the remodeled SGs and PBs and the VMs appears to be significant in that a significant proportion of the host mRNAs could have been sequestered in the SG-PB complexes by 4 hpi, setting the stage for hijacking the host translational machinery for selective translation of viral mRNAs. It is possible that sequestration and/or posttranslational modification of a large number of hnRNPs, ARE-BPs (11), and SG and PB proteins in the VM leads to suppression of some of their functions as well as cooption/modulation of the functions of some of the components to promote viral genome replication and virus assembly, in the absence of which the majority of the host proteins would negatively influence virus growth.

The demonstration in the present study that the rotavirus replication organelles represent a union of the triad of the viral replication complexes, SGs, and PBs as well as many hnRNPs, ARE-BPs, cytoplasmic proteins (11), and lipid droplets (19–21) adds

a new dimension to the compositional and structural complexity of the VM, signifying the need for a conceptual change in our current understanding of the composition of the VM and a rationalization for future strategies to unravel the structural organization of the supramolecular VM and the mechanism of morphogenesis of rotavirus.

MATERIALS AND METHODS

Cells and viruses. Embryonic African green monkey kidney-derived MA104 cells and transformed human embryonic kidney HEK293T cells were maintained in Dulbecco's modified Eagle's medium (DMEM) supplemented with 10% fetal bovine serum (FBS) (Invitrogen). Rhesus monkey rotavirus (RRV) and the human rotavirus strain KU were obtained from Harry B. Greenberg, Stanford University, USA. Infection, growth, and purification of viruses were done in medium lacking FBS as described by Dhillon et al. (11, 135). MA104 cells were used for large-scale virus culture, and HEK293T cells were used in experiments involving plasmid DNA or siRNA transfections followed by virus infection to study the effect of ectopic expression or downregulation of expression of the cellular proteins on virus growth.

Enzymes and reagents. Nucleotides, DNA purification kits, restriction endonucleases, T4 DNA ligase, and 2× PCR mix were from Fermentas. General laboratory chemicals were from Sigma-Aldrich, Promega, USA, and Merck, Germany. Oligonucleotides were obtained from Sigma-Aldrich or Eurofins, India.

Antibodies. In this study, MAbs and rabbit and guinea pig PAbs were used. Rabbit PAbs were used when appropriate MAbs against the host proteins were not available. The PAbs against host proteins obtained from commercial sources were examined for cross-reactivity with rotaviral proteins before their use in experiments, as described recently (11), and those that showed cross-reactivity to viral proteins in WB and ELISA were not used in this study. Anti-NSP5 and -NSP2 antibodies raised in guinea pigs were generously provided by O. Burrone, ICGEB, Trieste, Italy. The generation of anti-NSP5 and anti-NSP2 rabbit PAbs and their purification were described by Dhillon et al. (11). Rotavirus subgroup I (SGI) and subgroup II (SGII) DLP-specific MAbs were kindly provided by Harry B. Greenberg, Stanford University, USA. Anti-RRV DLP antibodies were generated in rabbits by use of purified DLPs (11, 135). PAbs against the host proteins Ago2 (sc32877), GW182 (sc66915), PKR (sc708), and p-eIF2α (sc101670) and MAbs against adenylate kinase (sc165981), guanylate kinase (sc365026), UMP-CMP kinase (sc376153), nucleotide diphosphate kinase nm23 (sc166677), GW182 (sc377006 and sc376939), DCP1a (sc100706), EDC4 (sc374211 and sc376382), p-eIF2α (sc293100), and Staufen (sc90992) were from Santa Cruz Biotechnologies. Rabbit PAbs against Caprin1 (HPA018126 and SAB1101135) and a goat anti-rabbit IgG–Alexa Fluor 488 secondary antibody (AP132JA4) were from Sigma-Aldrich. Rabbit PAbs against DCP1b (PA5-26885), DDX6 (PA5-27786), DCP1a (PA5-40931), ZBP1 (PA5-20455), CPEB (PA1-1100), EDC4 (PA5-30485), eIF2α (PA5-27660), PPM1A (PA5-29041), Staufen (PA5-28479), DDX6 (PA5-27786), and XRN1 (PA5-57110 and PA5-41888) and MAbs against p-eIF2α (MA5-15133), ADAR1 (MA5-17285), β-actin (MA5-15739), and β-tubulin (MA-16308) were from Thermo Fisher-Pierce. MAbs against Caf1-p150 (04-1522), Caf1-p60 (04-1523), PCNA (1742353), and LSM1 (MABE893) were obtained from Millipore. G3BP1 MAb (611126) was from BD Biosciences. PAbs against Pan3 (PA5-24880) and DCP1b (PA5-58894) and a goat anti-guinea pig IgG–Alexa Fluor 633 secondary antibody were obtained from Invitrogen. Donkey anti-rabbit IgG–horseradish peroxidase (HRP) conjugate (NA934v), sheep anti-mouse IgG–HRP conjugate (NA931v), goat anti-rabbit IgG–Cy5 conjugate (PA-45004), goat anti-mouse IgG–Cy3 conjugate (PA43002), and goat anti-rabbit IgG–Cy3 conjugate (PA-43004) secondary antibodies were from GE Healthcare. Details of other antibodies and use of the antibodies for WB and ICM were described previously by Dhillon et al. (11).

Transfections. HEK293T cells were transfected with plasmid DNAs (0.75 μg/well) by use of 2 μl of either X-treme DNA or X-treme siRNA transfection reagent and with siRNAs (30 pmol/well) by use of 3 μl X-treme siRNA transfection reagent (Roche Applied Science) in 24-well plates according to the supplier's protocol. Transfected cells were then infected with rotavirus between 36 and 48 hpi, depending on the experiment, as described by Dhillon et al. (11).

Plasmid vectors and cDNAs. The cDNAs (GenBank accession numbers) for G3BP1 (BC108278), Caprin1 (BC001731), CAF1-p60 (BC021218), CPEB1 (BC050629), ADAR1 (BC038227), DCP1a (BC007459), DDX6 (BC065007), EDC4 (BC064567), eIF2α (BC002513), and PKR (BC093676) were obtained from Thermo Fisher Scientific-Dharmacon. The open reading frames (ORFs) of these genes were amplified by PCR and were cloned as N-terminal fusions with the reporter mCherry, YFP, or ECFP in the pcDNA3.0 vector. The reporters were cloned between HindIII and BamHI or HindIII and EcoRI sites, and the cellular genes were cloned downstream of the reporters, between BamHI and XhoI or EcoRI and XhoI sites, depending on the gene. The codon-optimized reporter genes for expression in mammalian cells were from Clontech. The ORFs of DDX6, Caprin1, Caf1-p60, PKR, and TIA1 were cloned between BamHI and XhoI sites in the pGEX-4T2 vector, and those of eIF2α, HuR, and DCP1A between EcoRI and XhoI sites, for expression of the proteins in fusion with glutathione *S*-transferase (GST) in *Escherichia coli*. The viral proteins NSP2 and NSP5 from the IS2 human strain and the G3BP1 protein were expressed in fusion with an N-terminal histidine (NH) tag (11). NSP2 and NSP5 were also expressed in fusion with maltose-binding protein (MBP) and GST, respectively. Expression of hnRNPs in fusion with fluorescent proteins was described recently (11). Details of cloning of viral and cellular genes into expression vectors and purification of the proteins by affinity chromatography have been described previously (11, 135).

ICM. The growth of MA104 and HEK293T cells on glass coverslips in 6-well plates and virus infection, antibody staining, and image analysis methods were described recently by Dhillon et al. (11). Images were taken at a magnification of ×63 by use of LSM Zeiss 710 or LSM Zeiss 880 Airyscan confocal

microscopes. Anti-rabbit secondary antibodies tagged with Alexa Fluor 488 or Cy5 (emission at 670 nm; red), anti-mouse secondary antibody conjugated to Cy3 (emission at 570 nm; green), and anti-guinea pig secondary antibody conjugated to Alexa Fluor 633 (cyan) were used in this study at a dilution of 1:200 for detection of three different proteins simultaneously. Images were processed with Adobe Photoshop (Adobe Systems, Inc., San Jose, CA) and ImageJ freeware (http://rsb.info.nih.gov/ij/index.html) as described previously (11). Plotting of the plot profile curves and quantification of band intensities in Western blots were also carried out using ImageJ software. Fluorescence quantification of the ratios of cytoplasmic to nuclear abundances of proteins in the cells was done by calculating the corrected total cell fluorescence (CTCF) [using the formula CTCF = integrated density – (area of selected cell × mean fluorescence background reading)] and the cytoplasmic to nuclear fluorescence ratio for 50 virus-infected and 50 uninfected cells in each of three independent experiments, using ImageJ software. The normalized ratios from one experiment were plotted in the graphs next to the confocal images to show the relative fold changes, as recently described (11). Colocalization analyses to calculate Pearson's coefficients were performed on more than 50 infected cells per experiment by using Zen Black software (Carl Zeiss). Statistical analyses were performed using Student's *t* test.

Preparation of nuclear and cytoplasmic extracts and Western blotting. Preparation of nuclear and cytoplasmic fractions from serum-grown control MA104 cells, virus-infected cells, and mock-infected cells by use of an NE-PER nuclear cytoplasmic fractionation reagent kit (Thermo Scientific) and WB of the host and viral proteins were described previously by Dhillon et al. (11). For preparation of infected cell extracts, cells were infected at a multiplicity of infection (MOI) of 10. For study of the effects of host proteins and siRNAs on the level of viral protein expression by WB, HEK293T cells were infected at an MOI of 5.0.

ELIFA. Rotavirus titers in virus preparations and the effects of ectopic expression of cellular proteins and their downregulation of expression by siRNAs on the progeny virus yield were determined using an enzyme-linked immunoperoxidase focus assay (ELIFA) as previously described (11, 136). HEK293T cells were infected with 400 focus-forming units (FFU) per well in 24-well plates, and the progeny virus titers in MA104 cells were determined as described by Dhillon et al. (11).

ACKNOWLEDGMENTS

This work was supported by grants from SERB, Department of Science and Technology (grant SR/SO/BB-30/2010), and the Department of Biotechnology (grant BT/PR11549/MED/29/865/2014), Government of India, and by the DBT-IISc Partnership Program during 2011 to 2016. The Indian National Science Academy is acknowledged for an INSA senior scientist fellowship to C.D.R. P.D. has received Junior and Senior Research Fellowships from CSIR and a research associate fellowship from the Indian Institute of Science.

Services by the departmental and institutional confocal imaging facilities are acknowledged. We are grateful to M. A. McCrae, University of Warwick, United Kingdom, for his critical comments on the Ph.D. thesis of P.D. and for suggestions on the manuscript.

REFERENCES

1. Estes MK, Greenberg HB. 2013. Rotaviruses, p 1347–1401. *In* Knipe DM, Howley PM, Cohen JI, Griffin DE, Lamb RA, Martin MA, Racaniello VR, Roizman B (ed), Fields virology, 6th ed. Lippincott Williams & WilkinsPhiladelphia, PA.
2. Smith ML, Lazdins I, Holmes IH. 1980. Coding assignments of double-stranded RNA segments of SA11 rotavirus established by in vitro translation. J Virol 33:976–982.
3. Prasad BV, Wang GJ, Clerx JP, Chiu W. 1988. Three-dimensional structure of rotavirus. J Mol Biol 199:269–275. https://doi.org/10.1016/0022-2836(88)90313-0.
4. Settembre EC, Chen JZ, Dormitzer PR, Grigorieff N, Harrison SC. 2011. Atomic model of an infectious rotavirus particle. EMBO J 30:408–416. https://doi.org/10.1038/emboj.2010.322.
5. Estes MK, Cohen J. 1989. Rotavirus gene structure and function. Microbiol Rev 53:410–449.
6. Greenberg HB, McAuliffe V, Valdesuso J, Wyatt R, Flores J, Kalica A, Hoshino Y, Singh N. 1983. Serological analysis of the subgroup protein of rotavirus, using monoclonal antibodies. Infect Immun 39:91–99.
7. Fabbretti E, Afrikanova I, Vascotto F, Burrone OR. 1999. Two non-structural rotavirus proteins, NSP2 and NSP5, form viroplasm-like structures in vivo. J Gen Virol 80:333–339. https://doi.org/10.1099/0022-1317-80-2-333.
8. Contin R, Arnoldi F, Campagna M, Burrone OR. 2010. Rotavirus NSP5 orchestrates recruitment of viroplasmic proteins. J Gen Virol 91:1782–1793. https://doi.org/10.1099/vir.0.019133-0.
9. Eichwald C, Rodriguez JF, Burrone OR. 2004. Characterization of rotavirus NSP2/NSP5 interactions and the dynamics of viroplasm formation. J Gen Virol 85:625–634. https://doi.org/10.1099/vir.0.19611-0.
10. Patton JT, Silvestri LS, Tortorici MA, Vasquez-Del Carpio R, Taraporewala ZF. 2006. Rotavirus genome replication and morphogenesis: role of the viroplasm. Curr Top Microbiol Immunol 309:169–187.
11. Dhillon P, Tandra VN, Chorghade SG, Namsa ND, Sahoo L, Rao CD. 2018. Cytoplasmic relocalization and colocalization with viroplasms of host cell proteins, and their role in rotavirus infection. J Virol 92:e00612-18. https://doi.org/10.1128/JVI.00612-18.
12. Han SP, Tang YH, Smith R. 2010. Functional diversity of the hnRNPs: past, present and perspectives. Biochem J 430:379–392. https://doi.org/10.1042/BJ20100396.
13. Piñol-Roma S, Dreyfuss G. 1993. hnRNP proteins: localization and transport between the nucleus and the cytoplasm. Trends Cell Biol 3:151–155. https://doi.org/10.1016/0962-8924(93)90135-N.
14. Geuens T, Bouhy D, Timmerman V. 2016. The hnRNP family: insights into their role in health and disease. Hum Genet 135:851–867. https://doi.org/10.1007/s00439-016-1683-5.
15. Krecic AM, Swanson MS. 1999. hnRNP complexes: composition, structure, and function. Curr Opin Cell Biol 11:363–371. https://doi.org/10.1016/S0955-0674(99)80051-9.

16. Chen C-YA, Shyu A-B. 1995. AU-rich elements: characterization and importance in mRNA degradation. Trends Biochem Sci 20:465–470. https://doi.org/10.1016/S0968-0004(00)89102-1.
17. Barreau C, Paillard L, Osborne HB. 2005. AU-rich elements and associated factors: are there unifying principles? Nucleic Acids Res 33:7138–7150. https://doi.org/10.1093/nar/gki1012.
18. Baou M, Jewell A, Murphy JJ. 2009. TIS11 family proteins and their roles in posttranscriptional gene regulation. J Biomed Biotechnol 2009:634520. https://doi.org/10.1155/2009/634520.
19. Cheung W, Gill M, Sposito A, Kaminski CF, Courousse N, Chwetzoff S, Trugnan G, Keshavan N, Lever A, Desselberger U. 2010. Rotaviruses associate with cellular lipid droplet components to replicate in viroplasms, and compounds disrupting or blocking lipid droplets inhibit viroplasm formation and viral replication. J Virol 84:6782–6798. https://doi.org/10.1128/JVI.01757-09.
20. Gaunt ER, Zhang Q, Cheung W, Wakelam MJ, Lever AM, Desselberger U. 2013. Lipidome analysis of rotavirus-infected cells confirms the close interaction of lipid droplets with viroplasms. J Gen Virol 94:1576–1586. https://doi.org/10.1099/vir.0.049635-0.
21. Crawford SE, Desselberger U. 2016. Lipid droplets form complexes with viroplasms and are crucial for rotavirus replication. Curr Opin Virol 19:11–15. https://doi.org/10.1016/j.coviro.2016.05.008.
22. Campagna M, Eichwald C, Vascotto F, Burrone OR. 2005. RNA interference of rotavirus segment 11 mRNA reveals the essential role of NSP5 in the virus replicative cycle. J Gen Virol 86:1481–1487. https://doi.org/10.1099/vir.0.80598-0.
23. Mohan KV, Muller J, Som I, Atreya CD. 2003. The N- and C-terminal regions of rotavirus NSP5 are the critical determinants for the formation of viroplasm-like structures independent of NSP2. J Virol 77:12184–12192. https://doi.org/10.1128/JVI.77.22.12184-12192.2003.
24. López T, Rojas M, Ayala-Bretón C, López S, Arias CF. 2005. Reduced expression of the rotavirus NSP5 gene has a pleiotropic effect on virus replication. J Gen Virol 86:1609–1617. https://doi.org/10.1099/vir.0.80827-0.
25. Harding HP, Zhang Y, Bertolotti A, Zeng H, Ron D. 2000. Perk is essential for translational regulation and cell survival during the unfolded protein response. Mol Cell 5:897–904. https://doi.org/10.1016/S1097-2765(00)80330-5.
26. Wek SA, Zhu S, Wek RC. 1995. The histidyl-tRNA synthetase-related sequence in the eIF-2 alpha protein kinase GCN2 interacts with tRNA and is required for activation in response to starvation for different amino acids. Mol Cell Biol 15:4497–4506. https://doi.org/10.1128/MCB.15.8.4497.
27. Srivastava SP, Kumar KU, Kaufman RJ. 1998. Phosphorylation of eukaryotic translation initiation factor 2 mediates apoptosis in response to activation of the double-stranded RNA-dependent protein kinase. J Biol Chem 273:2416–2423. https://doi.org/10.1074/jbc.273.4.2416.
28. McEwen E, Kedersha N, Song B, Scheuner D, Gilks N, Han A, Chen JJ, Anderson P, Kaufman RJ. 2005. Heme-regulated inhibitor kinase-mediated phosphorylation of eukaryotic translation initiation factor 2 inhibits translation, induces stress granule formation, and mediates survival upon arsenite exposure. J Biol Chem 280:16925–16933. https://doi.org/10.1074/jbc.M412882200.
29. McCormick C, Khaperskyy DA. 2017. Translation inhibition and stress granules in the antiviral immune response. Nat Rev Immunol 17:647–660. https://doi.org/10.1038/nri.2017.63.
30. Kedersha N, Ivanov P, Anderson P. 2013. Stress granules and cell signalling: more than just a passing phase? Trends Biochem Sci 38:484–506.
31. Kimball SR, Horetsky RL, Ron D, Jefferson LS, Harding HP. 2003. Mammalian stress granules represent sites of accumulation of stalled translation initiation complexes. Am J Physiol Cell Physiol 284:C273–C284. https://doi.org/10.1152/ajpcell.00314.2002.
32. Kedersha N, Chen S, Gilks N, Li W, Miller IJ, Stahl J, Anderson P. 2002. Evidence that ternary complex (eIF2-GTP-tRNA(i)(Met))-deficient preinitiation complexes are core constituents of mammalian stress granules. Mol Biol Cell 13:195–210. https://doi.org/10.1091/mbc.01-05-0221.
33. Yamasaki S, Anderson P. 2008. Reprogramming mRNA translation during stress. Curr Opin Cell Biol 20:222–226. https://doi.org/10.1016/j.ceb.2008.01.013.
34. Kedersha N, Stoecklin G, Ayodele M, Yacono P, Lykke-Andersen J, Fritzler M, Scheuner D, Kaufman RJ, Golan RE, Anderson P. 2005. Stress granules and processing bodies are dynamically linked sites of mRNP remodelling. J Cell Physiol 169:871–884. https://doi.org/10.1083/jcb.200502088.
35. Tourriere H, Chebli K, Zekri L, Courselaud B, Blanchard JM, Bertrand E, Tazi J. 2003. The RasGAP-associated endoribonuclease G3BP assembles stress granules. J Cell Physiol 160:823–831. https://doi.org/10.1083/jcb.200212128.
36. Parker F, Maurier F, Delumeau I, Duchesne M, Faucher D, Debussche L, Dugue A, Schweighoffe ZF, Tocque B. 1996. A Ras-GTPase-activating protein SH3-domain-binding protein. Mol Cell Biol 16:2561–2569. https://doi.org/10.1128/MCB.16.6.2561.
37. Reineke LC, Dougherty JD, Pierre P, Lloyd RE. 2012. Large G3BP-induced granules trigger eIF2α phosphorylation. Mol Biol Cell 23:3499–3510. https://doi.org/10.1091/mbc.e12-05-0385.
38. Kedersha N, Panas MD, Achorn CA, Lyons S, Tisdale S, Hickman T, Thomas M, Lieberman J, McInerney GM, Ivanov P, Anderson P. 2016. G3BP-Caprin1-USP10 complexes mediate stress granule condensation and associate with 40S subunits. J Cell Physiol 212:845–860. https://doi.org/10.1083/jcb.201508028.
39. Reineke LC, Kedersha N, Langereis MA, van Kuppeveld FJ, Lloyd RE. 2015. Stress granules regulate double-stranded RNA-dependent protein kinase activation through a complex containing G3BP1 and Caprin1. mBio 6:e02486. https://doi.org/10.1128/mBio.02486-14.
40. Solomon S, Xu Y, Wang B, David MD, Schubert P, Kennedy D, Schrader JW. 2007. Distinct structural features of caprin-1 mediate its interaction with G3BP-1 and its induction of phosphorylation of eukaryotic translation initiation factor 2, entry to cytoplasmic stress granules, and selective interaction with a subset of mRNAs. Mol Cell Biol 27:2324–2342. https://doi.org/10.1128/MCB.02300-06.
41. Yang X, Shen Y, Garre E, Hao X, Krumlinde D, Cvijović M, Arens C, Nyström T, Liu B, Sunnerhagen P. 2014. Stress granule-defective mutants deregulate stress responsive transcripts. PLoS Genet 10:e1004763. https://doi.org/10.1371/journal.pgen.1004763.
42. Poblete-Duran N, Prades-Perez Y, Vera-Otarola J, Soto-Rifo R, Valiente-Echeverria F. 2016. Who regulates whom? An overview of RNA granules and viral infections. Viruses 8:180. https://doi.org/10.3390/v8070180.
43. Anderson P, Kedersha N. 2007. Stress granules: the Tao of RNA triage. Trends Biochem Sci 33:141–150. https://doi.org/10.1016/j.tibs.2007.12.003.
44. Ivanov P, Kedersha N, Anderson P. 2011. Stress puts TIA on TOP. Genes Dev 25:2119–2124. https://doi.org/10.1101/gad.17838411.
45. Fenger-Grøn M, Fillman C, Norrild B, Lykke-Andersen J. 2005. Multiple processing body factors and the ARE binding protein TTP activate mRNA decapping. Mol Cell 20:905–915. https://doi.org/10.1016/j.molcel.2005.10.031.
46. Stoecklin G, Anderson P. 2013. In a tight spot: ARE-mRNAs at processing bodies. Genes Dev 21:627–631. https://doi.org/10.1101/gad.1538807.
47. Onomoto K, Yoneyama M, Fung G, Kato H, Fujita T. 2014. Antiviral innate immunity and stress granule responses. Trends Immunol 35:420–428. https://doi.org/10.1016/j.it.2014.07.006.
48. Thomas MG, Loschi M, Desbats MA, Boccaccio GL. 2011. RNA granules: the good, the bad and the ugly. Cell Signal 23:324–334. https://doi.org/10.1016/j.cellsig.2010.08.011.
49. Anderson P, Kedersha N. 2009. RNA granules: post-transcriptional and epigenetic modulators of gene expression. Nat Rev Mol Cell Biol 10:430–436. https://doi.org/10.1038/nrm2694.
50. Reineke LC, Lloyd RE. 2013. Diversion of stress granules and P-bodies during viral infection. Virology 436:255–267. https://doi.org/10.1016/j.virol.2012.11.017.
51. Buchan JR, Parker R. 2009. Eukaryotic stress granules: the ins and outs of translation. Mol Cell 36:932–941. https://doi.org/10.1016/j.molcel.2009.11.020.
52. Anderson P, Kedersha N, Ivanov P. 2015. Stress granules, P-bodies and cancer. Biochim Biophys Acta 1849:861–870. https://doi.org/10.1016/j.bbagrm.2014.11.009.
53. Stoecklin G, Kedersha N. 2013. Relationship of GW/P-bodies with stress granules. Adv Exp Med Biol 768:197–211. https://doi.org/10.1007/978-1-4614-5107-5_12.
54. Chen CY, Shyu AB. 2011. Mechanisms of deadenylation-dependent decay. Wiley Interdiscip Rev RNA 2:167–183. https://doi.org/10.1002/wrna.40.
55. Goldstrohm AC, Wickens M. 2008. Multifunctional deadenylase complexes diversify mRNA control. Nat Rev Mol Cell Biol 9:337–344. https://doi.org/10.1038/nrm2370.

56. Whale E, Winkler GS. 2013. RNA decay machines: deadenylation by the Ccr4-Not and Pan2-Pan3 complexes. Biochim Biophys Acta 1829: 561–570. https://doi.org/10.1016/j.bbagrm.2013.01.003.
57. Ling SH, Qamra R, Song H. 2011. Structural and functional insights into eukaryotic mRNA decapping. Wiley Interdiscip Rev RNA 2:193–208. https://doi.org/10.1002/wrna.44.
58. Yu JH, Yang WH, Gulick T, Bloch KD, Bloch DB. 2005. Ge-1 is a central component of the mammalian cytoplasmic mRNA processing body. RNA 11:1795–1802. https://doi.org/10.1261/rna.2142405.
59. Dekanty A, Romero NM, Bertolin AP, Thomas MG, Leishman CC, Perez-Perri JI, Boccaccio GL, Wappner P. 2010. Drosophila genome-wide RNAi screen identifies multiple regulators of HIF-dependent transcription in hypoxia. PLoS Genet 6:e1000994. https://doi.org/10.1371/journal.pgen.1000994.
60. Cougot N, Bhattacharyya SN, Tapia-Arancibia L, Bordonné R, Filipowicz W, Bertrand E, Rage F. 2008. Dendrites of mammalian neurons contain specialized P-body-like structures that respond to neuronal activation. J Neurosci 28:13793–13804. https://doi.org/10.1523/JNEUROSCI.4155-08.2008.
61. Chahar HS, Chen S, Manjunath CN. 2013. P-body components LSM1, GW182, DDX3, DDX6 and XRN1 are recruited to WNV replication sites and positively regulate viral replication. Virology 436:1–7. https://doi.org/10.1016/j.virol.2012.09.041.
62. Castilla-Llorente V, Spraggon L, Okamura M, Naseeruddin S, Adamow M, Qamar S, Liu J. 2012. Mammalian GW220/TNGW1 is essential for the formation of GW/P bodies containing miRISC. J Cell Physiol 198: 529–544. https://doi.org/10.1083/jcb.201201153.
63. Yao B, La LB, Chen Y-C, Chang L-J, Chan EK. 2012. Defining a new role of GW182 in maintaining miRNA stability. EMBO Rep 13:1102–1108. https://doi.org/10.1038/embor.2012.160.
64. Eulalio A, Tritschler F, Izaurralde E. 2009. The GW182 protein family in animal cells: new insights into domains required for miRNA-mediated gene silencing. RNA 15:1433–1442. https://doi.org/10.1261/rna.1703809.
65. Huntzinger E, Kuzuoglu-Ozturk D, Braun JE, Eulalio A, Wohlbold L, Izaurralde E. 2013. The interactions of GW182 proteins with PABP and deadenylases are required for both translational repression and degradation of miRNA targets. Nucleic Acids Res 41:978–994. https://doi.org/10.1093/nar/gks1078.
66. Takimoto K, Wakiyama M, Yokoyama S. 2009. Mammalian GW182 contains multiple argonaute-binding sites and functions in microRNA-mediated translational repression. RNA 15:1078–1089. https://doi.org/10.1261/rna.1363109.
67. Beckham CJ, Parker R. 2008. P bodies, stress granules, and viral life cycles. Cell Host Microbe 3:206–212. https://doi.org/10.1016/j.chom.2008.03.004.
68. White JP, Lloyd RE. 2012. Regulation of stress granules in virus systems. Trends Microbiol 20:175–180. https://doi.org/10.1016/j.tim.2012.02.001.
69. Valiente-Echeverria F, Melnychuk L, Mouland AJ. 2012. Viral modulation of stress granules. Virus Res 169:430–437. https://doi.org/10.1016/j.virusres.2012.06.004.
70. Montero H, Rojas M, Arias CF, Lopez S. 2008. Rotavirus infection induces the phosphorylation of eIF2α but prevents the formation of stress granules. J Virol 82:1496–1504. https://doi.org/10.1128/JVI.01779-07.
71. Bhowmick R, Mukherjee A, Patra U, Chawla-Sarkar M. 2015. Rotavirus disrupts cytoplasmic P bodies during infection. Virus Res 210:344–354. https://doi.org/10.1016/j.virusres.2015.09.001.
72. Piotrowska J, Hansen SJ, Park N, Jamka K, Sarnow P, Gustin KE. 2010. Stable formation of compositionally unique stress granules in virus-infected cells. J Virol 84:3654–3665. https://doi.org/10.1128/JVI.01320-09.
73. Qin Q, Carroll K, Hastings C, Miller CL. 2011. Mammalian orthoreovirus escape from host translational shutoff correlates with stress granule disruption and is independent of eIF2alpha phosphorylation and PKR. J Virol 85:8798–8810. https://doi.org/10.1128/JVI.01831-10.
74. Roberts APE, Doidge R, Tarr AW, Jopling CL. 2014. The P body protein LSm1 contributes to stimulation of hepatitis C virus translation, but not replication, by microRNA-122. Nucleic Acids Res 42:1257–1269. https://doi.org/10.1093/nar/gkt941.
75. Yi Z, Pan T, Wu X, Song W, Wang S, Xu Y, Rice CM, Macdonald MR, Yuan Z. 2011. Hepatitis C virus co-opts Ras-GTPase-activating protein-binding protein 1 for its genome replication. J Virol 85:6996–7004. https://doi.org/10.1128/JVI.00013-11.
76. Emara MM, Brinton MA. 2007. Interaction of TIA-1/TIAR with West Nile and dengue virus products in infected cells interferes with stress granule formation and processing body assembly. Proc Natl Acad Sci U S A 104:9041–9046. https://doi.org/10.1073/pnas.0703348104.
77. Albornoz A, Carletti T, Corazza G, Marcello A. 2014. The stress granule component TIA-1 binds tick-borne encephalitis virus RNA and is recruited to perinuclear sites of viral replication to inhibit viral translation. J Virol 88:6611–6622. https://doi.org/10.1128/JVI.03736-13.
78. Pager CT, Schütz S, Abraham TM, Luo G, Sarnow P. 2013. Modulation of hepatitis C virus RNA abundance and virus release by dispersion of processing bodies and enrichment of stress granules. Virology 435: 472–484. https://doi.org/10.1016/j.virol.2012.10.027.
79. Khong A, Kerr CH, Yeung CH, Keatings K, Nayak A, Allan DW, Jan E. 2017. Disruption of stress granule formation by the multifunctional cricket paralysis virus 1A protein. J Virol 91:e01779-16. https://doi.org/10.1128/JVI.01779-16.
80. Nelson EV, Schmidt KM, Deflubé LR, Doğanay S, Banadyga L, Olejnik J, Hume AJ, Ryabchikova E, Ebihara H, Kedersha N, Ha T, Mühlberger E. 2016. Ebola virus does not induce stress granule formation during infection and sequesters stress granule proteins within viral inclusions. J Virol 90:7268–7284. https://doi.org/10.1128/JVI.00459-16.
81. Nie Y, Hammond GL, Yang JH. 2007. Double-stranded RNA deaminase ADAR1 increases host susceptibility to virus infection. J Virol 81: 917–923. https://doi.org/10.1128/JVI.01527-06.
82. Li Z, Wolff KC, Samuel CE. 2010. RNA adenosine deaminase ADAR1 deficiency leads to increased activation of protein kinase PKR and reduced vesicular stomatitis virus growth following interferon treatment. Virology 396:316–322. https://doi.org/10.1016/j.virol.2009.10.026.
83. Cachat A, Alais S, Chevalier SA, Journo C, Fusil F, Dutartre H, Boniface A, Ko NL, Gessain A, Cosset FL, Suspène R, Vartanian JP, Mahieux R. 2014. ADAR1 enhances HTLV-1 and HTLV-2 replication through inhibition of PKR activity. Retrovirology 11:93. https://doi.org/10.1186/s12977-014-0093-9.
84. Li Z, Liu G, Sun L, Teng Y, Guo X, Jia J, Sha J, Yang X, Chen D, Sun Q. 2015. PPM1A regulates antiviral signaling by antagonizing TBK1-mediated STING phosphorylation and aggregation. PLoS Pathog 11: e1004783. https://doi.org/10.1371/journal.ppat.1004783.
85. Xiang W, Zhang Q, Lin X, Wu S, Zhou Y, Meng F, Fan Y, Shen T, Xiao M, Xia Z, Zou J, Feng XH, Xu P. 2016. PPM1A silences cytosolic RNA sensing and antiviral defense through direct dephosphorylation of MAVS and TBK1. Sci Adv 2:e1501889. https://doi.org/10.1126/sciadv.1501889.
86. Sen A, Agresti D, Mackow ER. 2006. Hyperphosphorylation of the rotavirus NSP5 protein is independent of serine 67, NSP2, or the intrinsic insolubility of NSP5 and is regulated by cellular phosphatases. J Virol 80:1807–1816. https://doi.org/10.1128/JVI.80.4.1807-1816.2006.
87. Kobayashi T, Sadaie M, Ohnishi M, Wang H, Ikeda S, Hanada M, Yanagawa Y, Nakajima T, Tamura S. 1998. Isoform-specific phosphorylation of fission yeast type 2C protein phosphatase. Biochem Biophys Res Commun 251:296–300. https://doi.org/10.1006/bbrc.1998.9467.
88. Awano K, Amano K, Nagaura Y, Kanno S, Echigo S, Tamura S, Kobayashi T. 2008. Phosphorylation of protein phosphatase 2Czeta by c-Jun NH_2-terminal kinase at Ser92 attenuates its phosphatase activity. Biochemistry 47:7248–7255. https://doi.org/10.1021/bi800067p.
89. Dai F, Shen T, Li Z, Lin X, Feng XH. 2011. PPM1A dephosphorylates RanBP3 to enable efficient nuclear export of Smad2 and Smad3. EMBO Rep 12:1175–1181. https://doi.org/10.1038/embor.2011.174.
90. Chida T, Ando M, Matsuki T, Masu Y, Nagaura Y, Takano-Yamamoto T, Tamura S, Kobayashi T. 2013. N-myristoylation is essential for protein phosphatases PPM1A and PPM1B to dephosphorylate their physiological substrates in cells. Biochem J 449:741–749. https://doi.org/10.1042/BJ20121201.
91. Protter DSW, Parker R. 2016. Principles and properties of stress granules. Trends Cell Biol 26:668–679. https://doi.org/10.1016/j.tcb.2016.05.004.
92. Sfakianos AP, Whitmarsh AJ, Ashe MP. 2016. Ribonucleoprotein bodies are phased in. Biochem Soc Trans 44:1411–1416. https://doi.org/10.1042/BST20160117.
93. Kroschwald S, Maharana S, Mateju D, Malinovska L, Nüske E, Poser I, Richter D, Alberti S. 2015. Promiscuous interactions and protein disaggregases determine the material state of stress-inducible RNP granules. Elife 4:e06807. https://doi.org/10.7554/eLife.06807.
94. Lin Y, Protter DS, Rosen MK, Parker R. 2015. Formation and maturation of phase-separated liquid droplets by RNA-binding proteins. Mol Cell 60:208–219. https://doi.org/10.1016/j.molcel.2015.08.018.
95. Nott TJ, Petsalaki E, Farber P, Jervis D, Fussner E, Plochowietz A, Craggs

TD, Bazett-Jones DP, Pawson T, Forman-Kay JD, Baldwin AJ. 2015. Phase transition of a disordered nuage protein generates environmentally responsive membraneless organelles. Mol Cell 57:936–947. https://doi.org/10.1016/j.molcel.2015.01.013.
96. Van Treeck B, Protter DSW, Matheny T, Khong A, Link CD, Parker R. 2018. RNA self-assembly contributes to stress granule formation and defining the stress granule transcriptome. Proc Natl Acad Sci U S A 115:2734–2739. https://doi.org/10.1073/pnas.1800038115.
97. Khong A, Matheny T, Jain S, Mitchell SF, Wheeler JR, Parker R. 2017. The stress granule transcriptome reveals principles of mRNA accumulation in stress granules. Mol Cell 68:808–820. https://doi.org/10.1016/j.molcel.2017.10.015.
98. Martin D, Ouldali M, Menetrey J, Poncet D. 2011. Structural organisation of the rotavirus non-structural protein NSP5. J Mol Biol 413:209–221. https://doi.org/10.1016/j.jmb.2011.08.008.
99. Sen A, Sen N, Mackow ER. 2007. The formation of viroplasm-like structures by the rotavirus NSP5 protein is calcium regulated and directed by a C-terminal helical domain. J Virol 81:11758–11767. https://doi.org/10.1128/JVI.01124-07.
100. Afrikanova I, Fabbretti E, Miozzo MC, Burrone OR. 1998. Rotavirus NSP5 phosphorylation is up-regulated by interaction with NSP2. J Gen Virol 79:2679–2686. https://doi.org/10.1099/0022-1317-79-11-2679.
101. Arnoldi F, Campagna M, Eichwald C, Desselberger U, Burrone OR. 2007. Interaction of rotavirus polymerase VP1 with non-structural protein NSP5 is stronger than that with NSP2. J Virol 81:2128–2137. https://doi.org/10.1128/JVI.01494-06.
102. Torres-Vega MA, Gonzalez RA, Duarte M, Poncet D, Lopez S, Arias CF. 2000. The C-terminal domain of rotavirus NSP5 is essential for its multimerization, hyperphosphorylation and interaction with NSP6. J Gen Virol 81:821–830. https://doi.org/10.1099/0022-1317-81-3-821.
103. Eichwald C, Arnoldi F, Laimbacher AS, Schraner EM, Fraet C, Burrone OR, Ackerman M. 2012. Rotavirus viroplasm fusion and perinuclear localization are dynamic processes requiring stabilized microtubules. PLoS One 7:e47947. https://doi.org/10.1371/journal.pone.0047947.
104. Cabral-Romero C, Padilla-Noriega L. 2006. Association of rotavirus viroplasms with microtubules through NSP2 and NSP5. Mem Inst Oswaldo Cruz 101:603–611. https://doi.org/10.1590/S0074-02762006000600006.
105. Martin D, Duarte M, Lepault J, Poncet D. 2010. Sequestration of free tubulin molecules by the viral protein NSP2 induces microtubule depolymerisation during rotavirus infection. J Virol 84:2522–2532. https://doi.org/10.1128/JVI.01883-09.
106. Criglar JM, Hu L, Crawford SE, Hyser JM, Broughman JR, Prasad BVV, Estes MK. 2014. A novel form of rotavirus NSP2 and phosphorylation-dependent NSP2-NSP5 interactions are associated with viroplasm assembly. J Virol 88:786–798. https://doi.org/10.1128/JVI.03022-13.
107. Hu L, Chow DC, Patton JT, Palzkill T, Estes MK, Prasad BV. 2012. Crystallographic analysis of rotavirus NSP2-RNA complex reveals specific recognition of 5′ GG sequence for RTPase activity. J Virol 86:10547–10557. https://doi.org/10.1128/JVI.01201-12.
108. Tsai WC, Gayatri S, Reineke LC, Sbardella G, Bedford MT, Lloyd RE. 2016. Arginine demethylation of G3BP1 promotes stress granule assembly. J Biol Chem 291:22671–22685. https://doi.org/10.1074/jbc.M116.739573.
109. Gallouzi IE, Parker F, Chebli K, Maurier F, Labourier E, Barlat I, Capony JP, Tocque B, Tazi J. 1998. A novel phosphorylation-dependent RNase activity of GAP-SH3 binding protein: a potential link between signal transduction and RNA stability. Mol Cell Biol 18:3956–3965. https://doi.org/10.1128/MCB.18.7.3956.
110. Reineke LC, Tsai WC, Jain A, Kaelber JT, Jung SY, Lloyd RE. 2017. Casein kinase 2 is linked to stress granule dynamics through phosphorylation of the stress granule nucleating protein G3BP1. Mol Cell Biol 37:e00596-16. https://doi.org/10.1128/MCB.00596-16.
111. Tsai NP, Ho PC, Wei LN. 2008. Regulation of stress granule dynamics by Grb7 and FAK signalling pathway. EMBO J 27:715–726. https://doi.org/10.1038/emboj.2008.19.
112. Wippich F, Bodenmiller B, Trajkovska MG, Wanka S, Aebersold R, Pelkmans L. 2013. Dual specificity kinase DYRK3 couples stress granule condensation/dissolution to mTORC1 signaling. Cell 152:791–805. https://doi.org/10.1016/j.cell.2013.01.033.
113. Goulet I, Boisvenue S, Mokas S, Mazroui R, Côté J. 2008. TDRD3, a novel Tudor domain-containing protein, localizes to cytoplasmic stress granules. Hum Mol Genet 17:3055–3074. https://doi.org/10.1093/hmg/ddn203.
114. Ohn T, Kedersha N, Hickman T, Tisdale S, Anderson P. 2008. A functional RNAi screen links O-GlcNAc modification of ribosomal proteins to stress granule and processing body assembly. Nat Cell Biol 10:1224–1231. https://doi.org/10.1038/ncb1783.
115. Kwon S, Zhang Y, Matthias P. 2007. The deacetylase HDAC6 is a novel critical component of stress granules involved in the stress response. Genes Dev 21:3381–3394. https://doi.org/10.1101/gad.461107.
116. Leung AK, Vyas S, Rood JE, Bhutkar A, Sharp PA, Chang P. 2011. Poly(ADP-ribose) regulates stress responses and microRNA activity in the cytoplasm. Mol Cell 42:489–499. https://doi.org/10.1016/j.molcel.2011.04.015.
117. Blee TK, Gray NK, Brook M. 2015. Modulation of the cytoplasmic functions of mammalian post-transcriptional regulatory proteins by methylation and acetylation: a key layer of regulation waiting to be uncovered? Biochem Soc Trans 43:1285–1295. https://doi.org/10.1042/BST20150172.
118. Corcoran JA, Khaperskyy DA, McCormick C. 2011. Assays for monitoring viral manipulation of host ARE-mRNA turnover. Methods 55:172–181. https://doi.org/10.1016/j.ymeth.2011.08.005.
119. Dickson AM, Anderson JR, Barnhart MD, Sokoloski KJ, Oko L, Opyrchal M, Galanis E, Wilusz CJ, Morrison TE, Wilusz J. 2012. Dephosphorylation of HuR protein during alphavirus infection is associated with HuR relocalization to the cytoplasm. J Biol Chem 287:36229–36238. https://doi.org/10.1074/jbc.M112.371203.
120. Habelhah H, Shah K, Huang L, Ostareck-Lederer A, Burlingame AL, Shokat KM, Hentze MW, Ronai Z. 2001. ERK phosphorylation drives cytoplasmic accumulation of hnRNP-K and inhibition of mRNA translation. Nat Cell Biol 3:325–330. https://doi.org/10.1038/35060131.
121. Vassileva MT, Matunis MJ. 2004. SUMO modification of heterogeneous nuclear ribonucleoproteins. Mol Cell Biol 24:3623–3632. https://doi.org/10.1128/MCB.24.9.3623-3632.2004.
122. Liu Q, Dreyfuss G. 1995. In vivo and in vitro arginine methylation of RNA-binding proteins. Mol Cell Biol 15:2800–2808. https://doi.org/10.1128/MCB.15.5.2800.
123. García-Mauriño SM, Rivero-Rodríguez F, Velázquez-Cruz A, Hernández-Vellisca M, Díaz-Quintana A, De la Rosa MA, Díaz-Moreno I. 2017. RNA binding protein regulation and cross-talk in the control of AU-rich mRNA fate. Front Mol Biosci 4:71. https://doi.org/10.3389/fmolb.2017.00071.
124. Poncet D, Lindenbaum P, L'Haridon R, Cohen J. 1997. *In vivo* and *in vitro* phosphorylation of rotavirus NSP5 correlates with its localization in viroplasms. J Virol 71:34–41.
125. Campagna M, Marcos-Villar L, Arnoldi F, de la Cruz-Herrera CF, Gallego P, Gonzalez-Santamaria J, Gonzalez D, Lopitz-Otsoa F, Rodriguez MS, Burrone OR, Rivas C. 2013. Rotavirus viroplasm proteins interact with the cellular SUMOylation system: implications for viroplasm-like structure formation. J Virol 87:807–817. https://doi.org/10.1128/JVI.01578-12.
126. Sotelo PH, Schumann M, Krause E, Chnaiderman J. 2010. Analysis of rotavirus non-structural protein NSP5 by mass spectrometry reveals a complex phosphorylation pattern. Virus Res 149:104–108. https://doi.org/10.1016/j.virusres.2009.12.006.
127. Gonzalez SA, Burrone OR. 1991. Rotavirus NS26 is modified by addition of single O-linked residues of N-acetylglucosamine. Virology 182:8–16. https://doi.org/10.1016/0042-6822(91)90642-O.
128. Holloway G, Coulson BS. 2006. Rotavirus activates JNK and p38 signaling pathways in intestinal cells, leading to AP-1-driven transcriptional responses and enhanced virus replication. J Virol 80:10624–10633. https://doi.org/10.1128/JVI.00390-06.
129. Martin-Latil S, Cotte-Laffitte J, Beau I, Quéro AM, Géniteau-Legendre M, Servin AL. 2004. A cyclic AMP protein kinase A-dependent mechanism by which rotavirus impairs the expression and enzyme activity of brush border-associated sucrase-isomaltase in differentiated intestinal Caco-2 cells. Cell Microbiol 6:719–731. https://doi.org/10.1111/j.1462-5822.2004.00396.x.
130. Rossen JW, Bouma J, Raatgeep RH, Büller HA, Einerhand AW. 2004. Inhibition of cyclooxygenase activity reduces rotavirus infection at a postbinding step. J Virol 78:9721–9730. https://doi.org/10.1128/JVI.78.18.9721-9730.2004.
131. Sen A, Rott L, Phan N, Mukherjee G, Greenberg HB. 2014. Rotavirus NSP1 protein inhibits interferon-mediated STAT1 activation. J Virol 88:41–53. https://doi.org/10.1128/JVI.01501-13.
132. Kumar M, Jayaram H, Vasquez-del Caprio R, Jiang X, Taraporewala ZF, Jacobson RH, Patton JT, Prasad BV. 2007. Crystallographic and biochemical analysis of rotavirus NSP2 with nucleotides reveals a nucleo-

side diphosphate kinase-like activity. J Virol 81:12272–12284. https://doi.org/10.1128/JVI.00984-07.
133. Van Rompay AR, Johansson M, Karlsson A. 2000. Phosphorylation of nucleosides and nucleoside analogs by mammalian nucleoside monophosphate kinases. Pharmacol Ther 87:189–198. https://doi.org/10.1016/S0163-7258(00)00048-6.
134. Golden A, Benedict M, Shearn A, Kimura N, Leone A, Liotta LA, Steeg PS. 1992. Nucleoside diphosphate kinases, nm23, and tumor metastasis: possible biochemical mechanisms. Cancer Treat Res 63:345–358.
135. Jagannath MR, Kesavulu MM, Deepa R, Sastri PN, Kumar SS, Suguna K, Rao CD. 2006. N- and C-terminal cooperation in rotavirus enterotoxin: novel mechanism of modulation of the properties of a multifunctional protein by a structurally and functionally overlapping conformational domain. J Virol 80:412–425. https://doi.org/10.1128/JVI.80.1.412-425.2006.
136. Rao CD, Reddy H, Naidu JR, Raghavendra A, Radhika NS, Karande A. 2015. An enzyme-linked immune focus assay for rapid detection and enumeration, and a newborn mouse model for human non-polio enteroviruses associated with acute diarrhea. J Virol Methods 224:47–52. https://doi.org/10.1016/j.jviromet.2015.08.007.